Available online at www.sciencedirect.com

SciVerse ScienceDirect

Journal of the European Ceramic Society 32 (2012) 525–540

www.elsevier.com/locate/jeurceramsoc

Review

Oxide materials for high temperature thermoelectric energy conversion

Jeffrey W. Fergus *

Auburn University, Materials Research and Education Center, 275 Wilmore Laboratories, Auburn, AL 36849, USA

Received 12 July 2011; received in revised form 24 September 2011; accepted 1 October 2011
Available online 19 October 2011

Abstract

Thermoelectric energy conversion can be used to capture electric power from waste heat in a variety of applications. The materials that have been shown to have the best thermoelectric properties are compounds containing elements such as tellurium and antimony. These compounds can be oxidized if exposed to the high temperature air that may be present in heat recovery applications. Oxide materials have better stability in oxidizing environments, so their use enables the fabrication of more durable devices. Thus, although the thermoelectric properties of oxides are inferior to those of the compounds mentioned above, their superior stability may expand potential the high temperature application of thermoelectric energy conversion.

In this paper, the thermoelectric properties of promising oxide materials are reviewed. The different types of oxides used for thermoelectric applications are compared and approaches for improving performance through doping are discussed.

Keywords: B. Electrical conductivity; B. Thermal conductivity; Seebeck coefficient

Contents

1. Introduction

Thermoelectric devices allow for the direct conversion of heat to electrical energy. The absence of any moving parts, such as pumps or compressors, makes thermoelectric conversion devices especially attractive for remote applications where repair is difficult or impossible. The ultimate remote application is for spacecraft, such as Cassini or Galileo, which have traveled so far from the sun that solar energy is insufficient to power the control, data collection and communication systems. In these spacecraft electrical power is provided by radioisotope thermoelectric generators (RTGs), which convert the heat generated by a radioactively decaying material into electrical energy.[1] Similar devices have been used in remote terrestrial locations, such as light houses or beacons, but are being decommissioned due environmental concerns.[2]

* Tel.: +1 334 844 3405; fax: +1 334 844 3400.
E-mail address: jwfergus@eng.auburn.edu

0955-2219/$ – see front matter © 2011 Elsevier Ltd. All rights reserved.
doi:10.1016/j.jeurceramsoc.2011.10.007

Increases in global energy consumption and the negative environmental impacts of many current energy conversion technologies, such as the combustion of fossil fuels, has led to increased activity in developing alternative energy conversion technologies. Although thermoelectric energy conversion devices are not likely to replace current primary power generation devices, they can provide supplemental conversion to improve overall system efficiencies. In particular, thermoelectric devices can be used to convert waste heat into electrical energy. One promising application is in automobiles where heat lost in the engine coolant or exhaust gas can be converted into electrical energy.[3–6] There are also potential applications in woodstove[6] and diesel[7] power plants where thermoelectric recovery of energy in waste heat can improve system efficiency.

A major challenge in the implementation of thermoelectric power generation is the low energy conversion efficiency. The voltage generated by a thermoelectric material placed in a temperature gradient is related to the thermopower (or Seebeck coefficient), which should be large. Electrical current must pass through the thermoelectric material, so its electrical conductivity should be high to minimize ohmic losses. At the same time, the thermal conductivity of the material should be low, so that a large thermal gradient is maintained. These three requirements are captured in the dimensionless figure of merit (ZT), which is given by

$$ZT = \left(\frac{\sigma S^2}{\kappa}\right) T \tag{1}$$

where σ is the electrical conductivity, S is the Seebeck coefficient, κ is the thermal conductivity and T is temperature.[8,9] Although the optimal properties may be different for different operating conditions and device designs, the figure of merit provides a basis for comparing materials. One of the challenges in increasing the figure of merit is that improvements resulting from changes in one property are often offset by changes in another property. For example, metals have high electrical conductivity, but small Seebeck coefficients and high thermal conductivity, while thermal insulators are typically also electrical insulators. In particular, heat is conducted through a solid by electron conduction and lattice phonon conduction. The electron contribution (κ_e) is related directly to the electronic conductivity (σ) according to the Wiedemann–Franz relationship which indicates that the ratio of the two properties is constant at a given temperature according to the following relation,[10]

$$\frac{\kappa_e}{\sigma} = \left(\frac{\pi^2 k_B^2}{3e^2}\right) T \tag{2}$$

where k_B is Boltzmann's constant, and e is the charge of an electron, so any improvement in electronic conductivity leads to an offsetting increase in the electronic contribution to the thermal conductivity. Thus, materials in which thermal conduction is dominated by lattice phonon contributions are more promising for thermoelectric application, since the phonon thermal conduction can be decreased without decreasing the electrical conduction.[10,11]

One specific approach to decreasing thermal conductivity is to use complex structures that increase the optical phonon modes. Similarly, structures with weakly bound or out-of-site atoms can create rattling modes, which interfere with the heat conduction. Doping with large atoms can also be used to decrease the thermal conductivity without decreasing electrical conductivity. These and other approaches have been used to improve the thermoelectric performance of materials.

The largest figures of merit have been achieved with tellurium-, antimony- and germanium-based compounds.[3,11–16] A figure of merit of one or larger is generally considered to be needed for practical applications and many of these compounds exceed that requirement. However, the stability and toxicity of these compounds is an issue for some applications. There are some oxides of less toxic elements that are promising for use in thermoelectric devices. The figures of merit for these materials are generally inferior to those of the skutterudites and other compounds mentioned above, but the stability is better and the negative environmental impact is less. If the durability can be improved and the cost decreased, such oxide thermoelectric materials may be used in devices for harvesting energy from waste heat.

The objective of this paper is to review the current status of oxide thermoelectric materials. The paper includes a compilation of results from the literature on the thermoelectric properties of promising n-type and p-type oxide materials. For the general classes of materials, the three important properties (electrical conductivity, thermopower and thermal conductivity) are presented and used to calculate the figure of merit. In addition, the effects of compositional changes on these properties and the on the figure of merit are discussed.

2. p-Type oxides

2.1. Layered cobaltites

The most promising p-type oxide thermoelectric materials are those based on alkali or alkaline-earth cobaltite compounds that form layered structures.[10,13,16] These compounds have large Seebeck coefficients, which is attributed to the low spin state of Co^{3+}.[17] Variations in cobalt valence, as evidenced by the changes in oxygen content, have been reported to affect the thermoelectric properties of $Ca_3Co_4O_9$.[18] The structures contain CoO_2 planes, which provide a path for p-type electronic conduction, while the interfaces between these layers and the other structural components disrupt heat transfer by lattice phonons. The structures for two promising thermoelectric oxides $Ca_3Co_4O_9$[13,19–24] and Na_xCoO_2[25–28] are shown schematically in Fig. 1. In $Ca_3Co_4O_9$, the CoO_2 planes are separated by a Ca_2CoO_3 layer that forms a rock salt type structure (Fig. 1a), while in Na_xCoO_2, the CoO_2 layers are separated by a layer of sodium ions (Fig. 1b). Calcium can also form Ca_xCoO_2[29] as well as $Ca_3Co_2O_6$.[30] Although $Ca_3Co_2O_6$ has a large Seebeck coefficient, the conductivity is low, so $Ca_3Co_4O_9$ has been more widely used for thermoelectric applications.

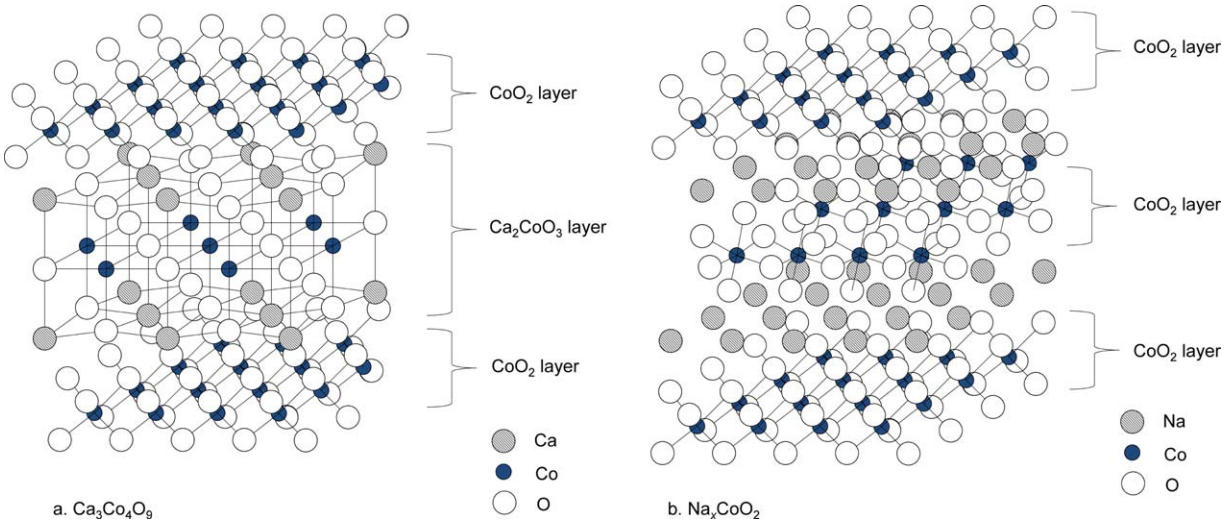

Fig. 1. Schematic structure of $Ca_3Co_4O_9$(a)[13,19–24] and Na_xCoO_2(b).[25–28]

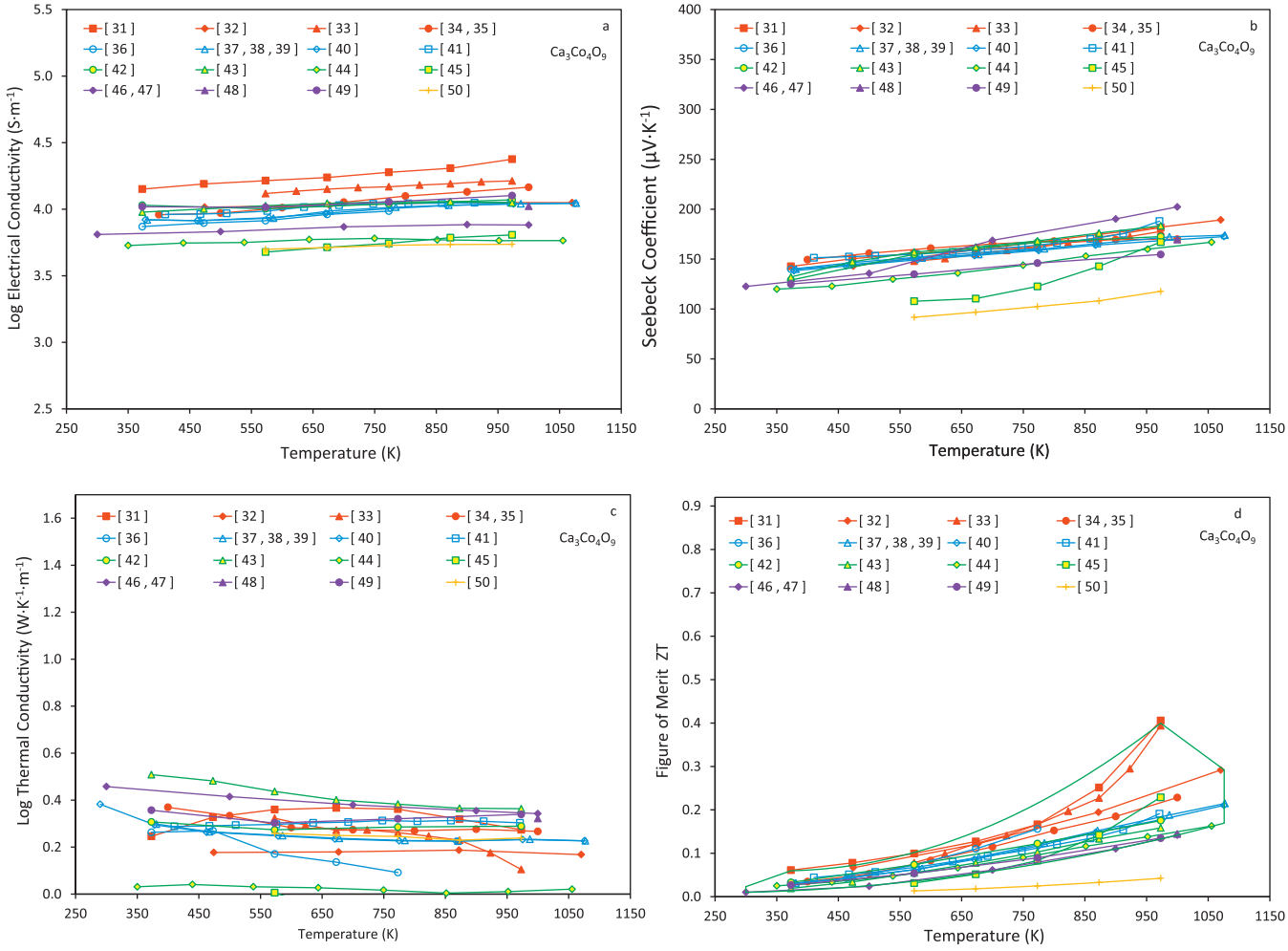

Fig. 2. Electrical conductivity (a), Seebeck coefficient (b), thermal conductivity (c) and figure of merit (*ZT*) (d) for $Ca_3Co_4O_9$.[31–50]. (For interpretation of the references to color in this artwork, the reader is referred to the web version of this article.)

2.1.1. $Ca_3Co_4O_9$

The thermoelectric properties of $Ca_3Co_4O_9$ are summarized in Fig. 2.[31–50] The results from various studies are fairly consistent with a conductivity of around 10^4 S m^{-1}, a Seebeck coefficient of around 150 μV K^{-1} and a thermal conductivity of around 2 W K^{-1} m^{-1}. In Fig. 2d, a line representing the range of most of the values of figure of merit is shown and will be used in subsequent plots to show the effects of dopant additions.

One dopant commonly used with $Ca_3Co_4O_9$ is bismuth, which has been shown to increase both the electrical conductivity and Seebeck coefficient[42,45,50–55] as well as decrease the thermal conductivity.[42,45,50] The increase in conductivity is attributed to an increase in carrier mobility[42,51,52] rather than carrier concentration, which is generally desired in thermoelectric materials, since an increase in carrier concentration tends to lead to a decrease in the Seebeck coefficient. However, improvements in the conductivity have also been attributed to differences in the microstructure.[53] The decrease in thermal conductivity has been attributed to the larger size and mass of bismuth as compared to calcium.[50] The figures of merit of $Ca_3Co_4O_9$ doped with bismuth and other ions are shown in Fig. 3a.[37,38,41,42,45–47,50,54,56,57] Although bismuth additions have been shown to improve all three properties contributing to the figure of merit, the reported figures of merit are in middle to upper range of those reported for undoped $Ca_3Co_4O_9$.

The addition that appears to have the greatest impact on the figure of merit is silver, which can be added as a dopant or as a second (metallic) phase. As a dopant, silver has been shown to increase the electrical conductivity,[41,57–60] which has been attributed to an increase in carrier concentration and mobility.[57–59] The addition of silver has been shown to either increase[57,58,60] or decrease the Seebeck coefficient.[59] In addition, observed decreases in the thermal conductivity have been attributed to the large mass of silver.[57,58] Silver has also been shown to increase electrical conductivity as a co-dopant with barium[41,61] or lutetium.[39] The presence of silver as a second phase also increases the electrical conductivity, but, in contrast to its use as a dopant, leads to a decrease in the Seebeck coefficient.[51,57,60,62,63] When combined with a dopant, however, the silver second phase can lead to an increase in both electrical conductivity and thermopower.[19,51,64,65]

Also shown in Fig. 3a are results for $Ca_3Co_4O_9$ doped with transition metals. Copper, when replacing cobalt, is consistently reported to increase the electrical conductivity, but also to decrease the Seebeck coefficient.[46,53,66,67] Copper is reported to occupy sites in the Ca_2CoO_3 rock salt layer rather than the CoO_2 layer of $Ca_3Co_4O_9$.[46] There is one report in which copper was used to replace calcium, rather than cobalt, and led to an increase in the Seebeck coefficient.[68] However, X-ray diffraction results showed the presence of a second phase, which suggests that copper is not stable on the calcium sites and the properties may be affected by the second phase. Other transition metal dopants, such as iron and manganese, occupy cobalt sites in the CoO_2 layer.[46] Although there are reports of increases in electrical conductivity due to doping of iron[46] or nickel,[67] in most cases the beneficial effect of transition metal dopants is an increase in thermopower, rather than increase in electrical conductivity, as in doping with either titanium,[47] manganese,[46,66] nickel[66] or iron.[66,67] Heavier transition metal dopants used include rhodium, which increases electrical conductivity, but decreases thermopower[69] and tantalum, which, conversely, increases thermopower, but decreases the electrical conductivity.[24] Additions of lead or gallium, like bismuth, increase both the electrical conductivity and thermopower.[24] Gallium also decreases thermal conductivity and has a figure of merit in the upper range of those shown in Fig. 3a.[37,38]

The figures of merit of $Ca_3Co_4O_9$ doped with other dopants are shown in Fig. 3b.[34,35,40,43,44,48,49,70–74] The results reported for lanthanum doping are mixed in that both increases in thermopower and decreases in electrical conductivity[75] as well as the opposite trends (increase in electrical conductivity and decrease in thermopower)[76] have been reported. However, reports for other lanthanide elements are consistent in that the addition of neodymium,[77] europium,[34] holmium,[40] dysprosium,[40] erbium,[40] ytterbium[78] and lutetium[40] lead to an increase in thermopower, but a decrease in electrical conductivity. Yttrium additions have a similar effect in increasing thermopower and decreasing electrical conductivity.[49] Additions of gadolinium, dysprosium, holmium and ytterbium have been shown to lead to a decrease in thermal conductivity.[79] Fig. 3b shows that the figures of merit for the lanthanide doped materials are in the same range as those for undoped $Ca_3Co_4O_9$.

Sodium additions have been shown to increase the conductivity for both $Ca_3Co_4O_9$[54,80] and $Ca_3Co_2O_6$.[67] The increase in Seebeck coefficient of $Ca_3O_4O_9$ with sodium additions alone is small[54,80] but can be increased by co-doping with manganese.[81] Co-doping of sodium with neodymium can also lead to an increase in thermopower, as well as a decrease in thermal conductivity, but in this case the electrical conductivity is decreased.[71] Like sodium, potassium additions to $Ca_3O_4O_9$ lead to an increase in electrical conductivity with only a slight increase in Seebeck coefficient and an increase in thermal conductivity, the net result of which is a modest increase in the figure of merit.[44,75] Co-doping of potassium with lanthanum has been shown to increase the electrical conductivity without significantly affecting the Seebeck coefficient.[75]

Barium additions have been shown to lead to a decrease in both electrical conductivity and thermopower in some cases[41,61] but also to an increase in figure of merit in another study.[31] The latter study showed a significant effect of processing conditions on the measured properties, so it is possible that microstructural differences may contribute to the observed effects of barium additions. Although $Sr_3Co_4O_9$ has a lower conductivity than $Ca_3Co_4O_9$, small strontium additions to $Ca_3Co_4O_9$ do not significantly affect the electrical conductivity, but lead to a decrease in thermal conductivity and thus a small increase in the figure of merit.[48]

A related structure with the general formula $Bi_2RE_2Co_{1.7-2}O_x$ (RE = Ca or Sr), which contains an expansion of the rock salt layer present in $Co_3O_4O_9$, can form.[23,74] Although the superlattice structure does lead to relatively low thermal conductivities of ~0.8 and ~1.2 W K^{-1} m^{-1} for $Bi_2Ca_2Co_{1.7}O_x$[73] and $Bi_2Sr_{1.94}La_{0.06}Co_2O_9$,[74] respectively,

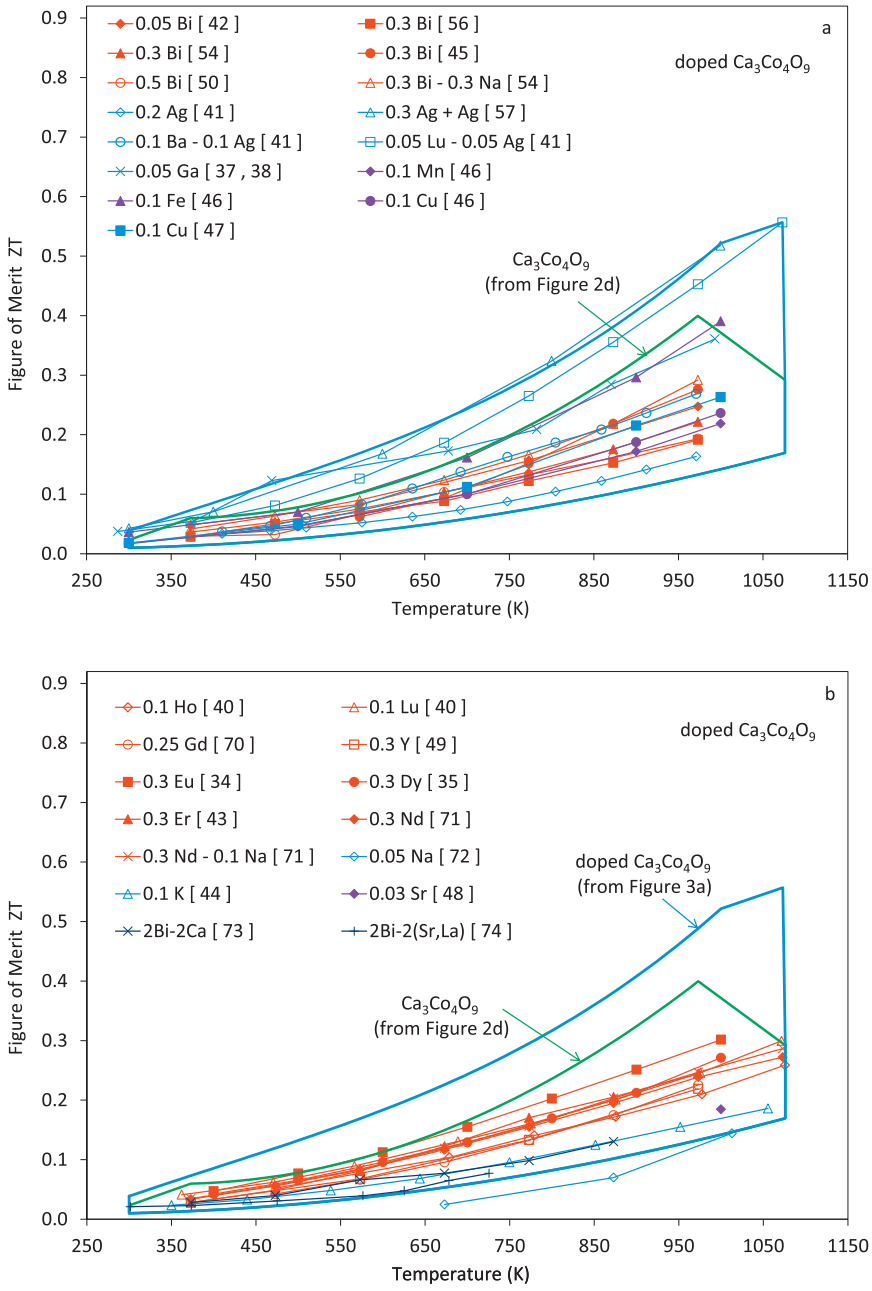

Fig. 3. Figure of merit (*ZT*) for doped $Ca_3Co_4O_9$.[34,35,37,38,40–50,54,56,57,70–74]. (For interpretation of the references to color in this artwork, the reader is referred to the web version of this article.)

the figure of merit is relatively low as compared to $Ca_3Co_4O_9$ (see 2Bi–2Ca and 2Bi–2(Sr, La) in Fig. 3b).

2.1.2. Na_xCoO_2

Another important layered cobaltite based thermoelectric material is Na_xCoO_2, the properties of some examples of which are summarized in Fig. 4.[82–86] The variation in the properties of Na_xCoO_2 is large as compared to the variation in $Co_3Co_4O_9$. One reason for this variation is that the sodium content differs between reports and the transport properties are affected by the concentration of sodium ion vacancies. The electrical conductivity has been shown to increase with sodium content up to 0.75–0.78.[87,88] In general, however, the electrical conductivities of Na_xCoO_2 are higher than those of $Co_3Co_4O_9$ (compare Figs. 2 and 4a).

As with $Co_3Co_4O_9$ the addition of silver improves the thermoelectric properties of Na_xCoO_2. Silver doping has been shown to increase electrical conductivity and thermopower[27,89,90] as well as to decrease thermal conductivity.[90] Silver as a second phase also increases electrical conductivity and thermopower, but increases thermal conductivity, so the figure of merit is not changed significantly.[86,91]

Copper[92,93] and zinc[94,95] additions to Na_xCoO_2 have been shown to increase the electrical conductivity and thermopower,

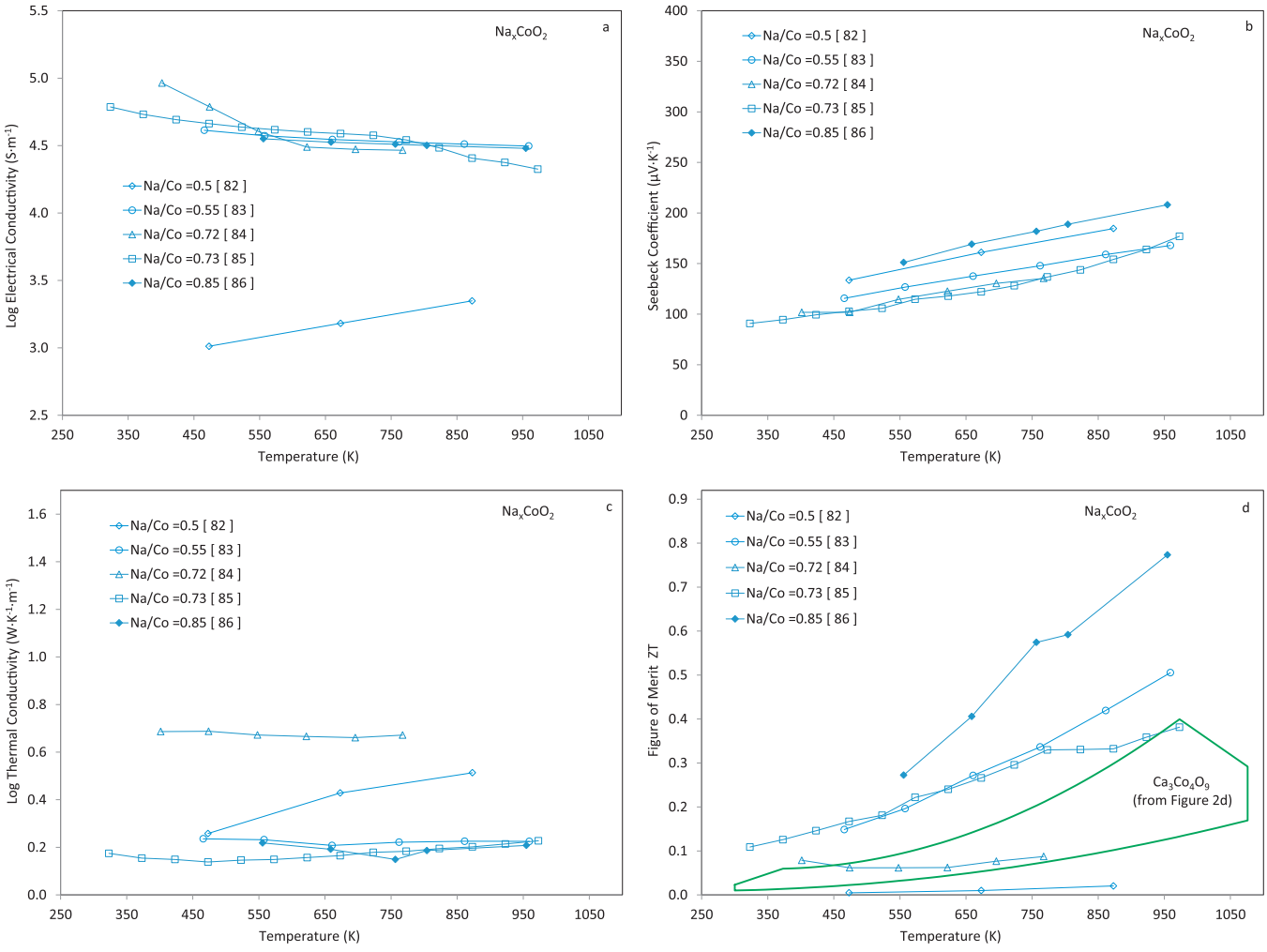

Fig. 4. Electrical conductivity (a), Seebeck coefficient (b), thermal conductivity (c) and figure of merit (*ZT*) (d) for Na_xCoO_2.[82–86]

while nickel increases the thermopower, but decreases the electrical conductivity.[84,93,96] When nickel and copper are added together the conductivity decreases.[93]

The effects of other dopants on the figure of merit of Na_xCoO_2 are summarized in Fig. 5.[83,84,86] In general, the figures of merit for the doped materials are similar to those of the corresponding undoped material. The largest difference in Fig. 5 is for nickel doping, but that difference was due, at least in part, to differences in the grain sizes of the materials.[84] Potassium additions have little effect on the properties of Na_xCoO_2,[83] but strontium leads to an increase in electrical conductivity and in the figure of merit.[83] In one study, the addition of some lanthanide elements (neodymium. samarium, ytterbium) and yttrium have been shown to decrease both thermal and electrical conductivity with little effect on the figure of merit.[83] There are reports of lanthanide additions increasing the power factor (σS^2) by increasing the Seebeck coefficient with ytterbium[97] or the electrical conductivity with dysprosium,[97] but the thermal conductivity was not reported, so the effect on the figure of merit cannot be determined.

The figure of merit of Na_xCoO_2 varies considerable, but is often higher than that of $Co_3Co_4O_9$. However, $Co_3Co_4O_9$ is more commonly used in thermoelectric devices due to its superior stability to compositional changes as compared to Na_xCoO_2,[98,99] which, as shown above, affect the thermoelectric properties.

2.2. *Other p-type oxides*

$LaCoO_3$ doped on the lanthanum site (*e.g.* strontium[100]) or cobalt site (*e.g.* nickel[101,102] or rhodium[103]) or both sites (strontium and rhodium[104]) has been reported as a thermoelectric material, but the figures of merit at high temperatures are relatively low (~0.01–0.1).Similarly, doped $LaCuO_4$ materials have good thermoelectric properties at low temperatures but low figures of merit at high temperatures.[105] $CuAlO_2$ doped with magnesium,[106] silver[107] or silver and zinc[107] have been investigated, but the figures are also small (~0.03–0.14).

3. n-Type oxides

3.1. *$SrTiO_3$*

Strontium titanate is a good electronic conductor when doped with higher valence ions (*i.e.* electron donors). The thermoelectric properties for one of the more common dopants, lanthanum

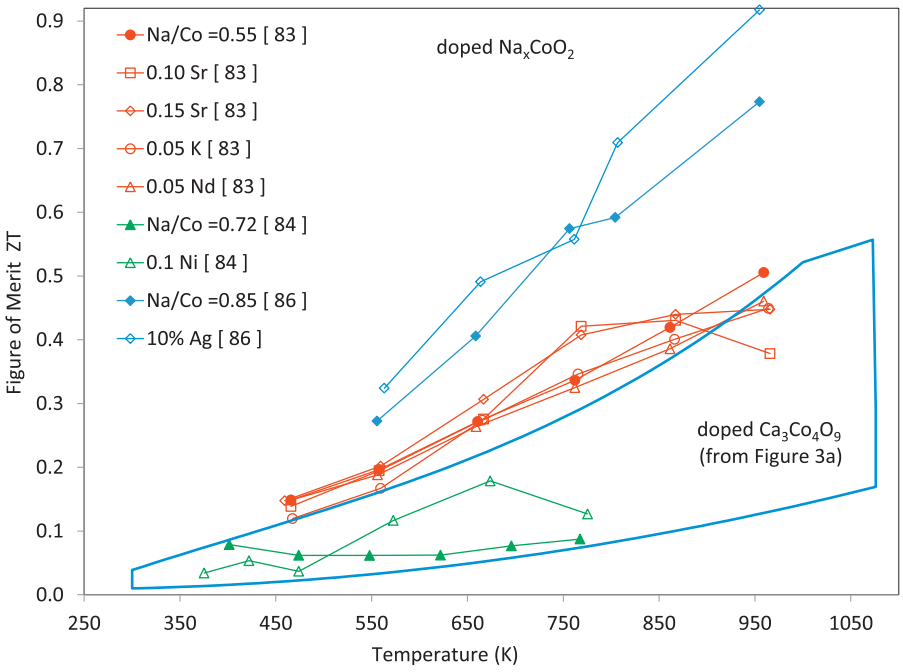

Fig. 5. Figure of merit (*ZT*) for doped Na_xCoO_2.[83,84,86]

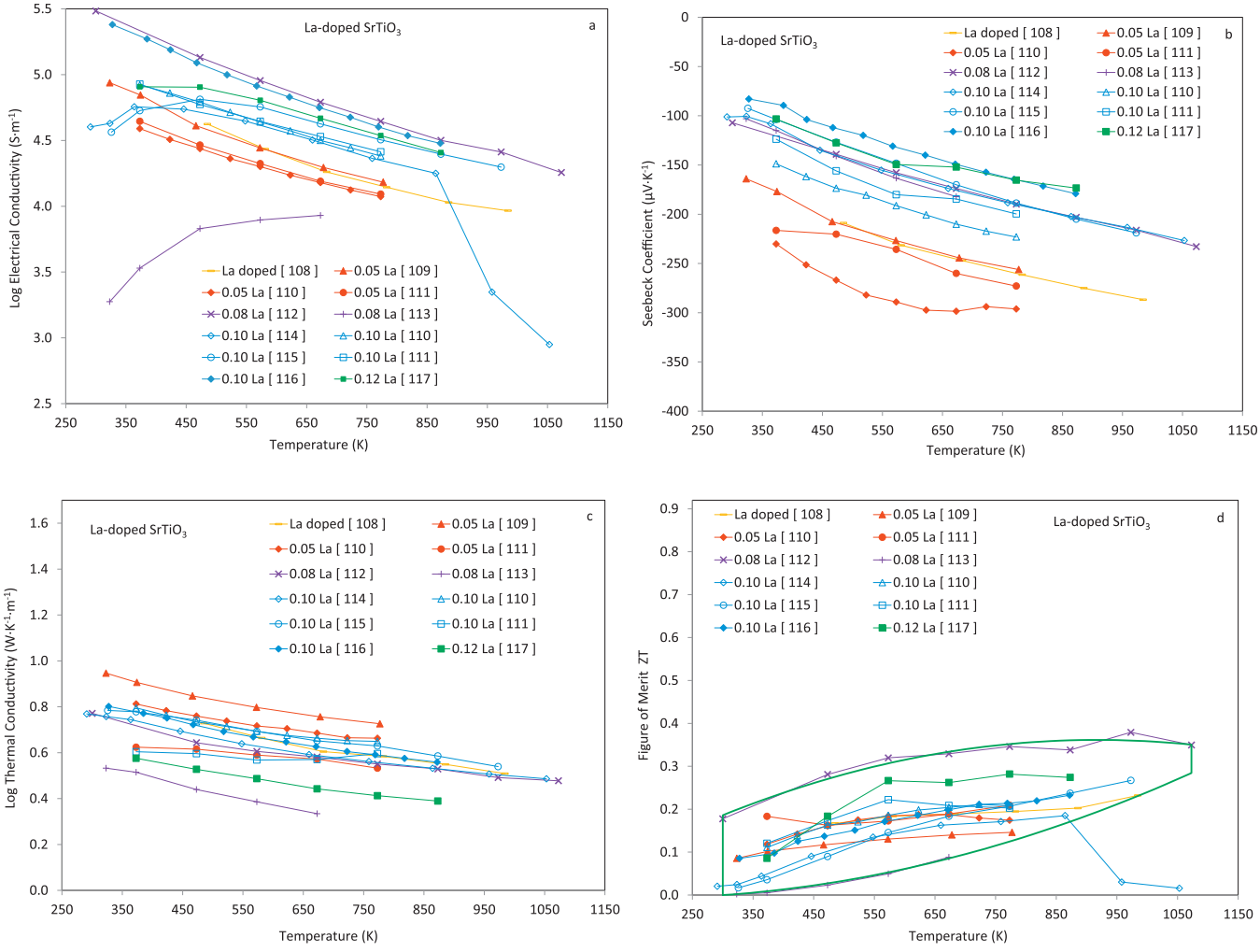

Fig. 6. Electrical conductivity (a), Seebeck coefficient (b), thermal conductivity (c) and figure of merit (*ZT*) (d) for La-doped $SrTiO_3$.[108–117]

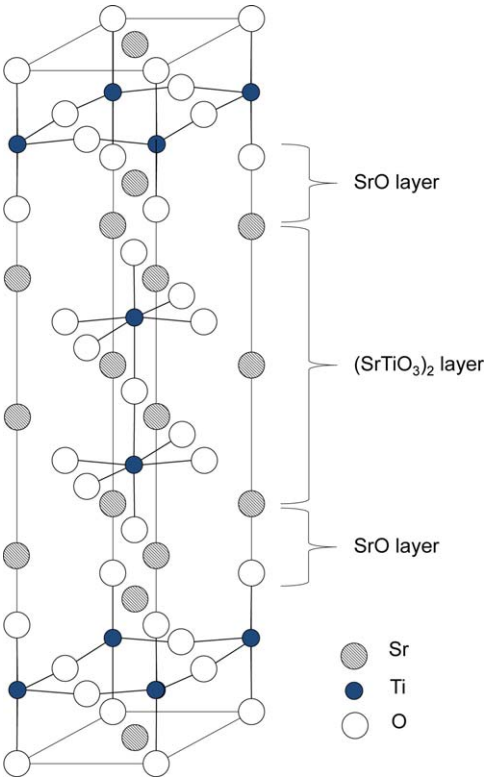

Fig. 7. Schematic structure of Ruddlesden–Popper (SrO) $(SrTiO_2)_n$ ($n = 2$).[121–123]

replacing strontium, are summarized in Fig. 6.[108–117] The addition of lanthanum increases electrical conductivity[108,110,111,118] and Seebeck coefficient[110,111,119] with only small changes in thermal conductivity[108,110,111] and thus improves the figure of merit. The conductivities (electrical and thermal) of strontium titanate are higher than those of p-type layer cobaltites discussed above (compare Figs. 2 and 6a and d).

Strontium titanate forms the perovskite crystal structure, but when doped can form a superlattice Ruddlesden–Popper structure, which offers a potential mechanism for reducing thermal conductivity as in layered cobaltites.[120] The Ruddlesden–Popper structure, $(SrO)(SrTiO_3)_n$ or $Sr_{n+1}Ti_nO_{3n+1}$, for $n = 2$, is shown schematically in Fig. 7, and consists of perovskite layers separated by SrO layers.[121–123] The formation of the Ruddlesden–Popper phase does lead to the desired decrease in thermal conductivity, but also leads to a decrease in electrical conductivity, which limits the impact on the figure or merit.[124] The figure of merit for one Ruddlesden–Popper compound, $(Sr_{0.95}Gd_{0.05})_3Ti_2O_7$(labeled 0.05 Gd, $n = 2$), is shown in Fig. 8 along with several other strontium titanate based materials[108,114,122,123,125–129], and is in the lower range of the values for $(La,Sr)TiO_3$. Similarly, for a neodymium-doped strontium titanate, $(Sr_{1-x}Nd_x)_{n+1}Ti_nO_{3n+1}$, the figure of merit for $n = 2$ is higher than that for $n = 1$, the latter of which would contain more SrO-perovskite interfaces per volume.[120] These results suggest that the layered structure is not as effective for increasing the figure of merit as for the cobaltite systems.

Other lanthanides have been used to dope strontium titanate. A comparison of several lanthanide dopants has shown that dysprosium results in the highest figure of merit.[114] When co-doping with lanthanum, replacement of strontium with dysprosium leads to an increase in electrical conductivity, increase in Seebeck coefficient and decrease in thermal conductivity,[130] but if the dysprosium replaces lanthanum, the conductivity and Seebeck coefficient decrease.[131] Yttrium has beneficial effects by increasing the Seebeck coefficient.[118,132–134]

Niobium addition leads to an increase in electrical conductivity[108,125,135] with similar[125] or lower Seebeck coefficients.[119,135,136] The effect of niobium on the thermal conductivity is varied as increases[119], decreases[13] or no significant changes[108,125] have been reported.

The addition of potassium titanate (KTO) has been shown to increase the electrical conductivity and decrease the thermal conductivity, which results in a good figure of merit as shown in Fig. 8.[127] The lanthanum-doped barium titanate–strontium titanate solid solution has been evaluated for its thermoelectric properties and a composition containing 30% barium (*i.e.* $Ba_{0.3}Sr_{0.6}La_{0.1}TiO_3$) was shown to have the best performance.[116]

3.2. $CaMnO_3$

Another promising n-type oxide for thermoelectric applications is $CaMnO_3$. Like $SrTiO_3$, $CaMnO_3$ is typically doped and can be doped on either site. The thermoelectric properties of $CaMnO_3$ with two common dopants, ytterbium on the calcium site and niobium on the manganese site, are summarized in Fig. 9.[105,137–143] Ytterbium doping leads to higher electrical conductivity and Seebeck coefficient, which results in a larger figure of merit. As compared to $SrTiO_3$, $CaMnO_3$ has a lower conductivity, both thermal (compare Figs. 6 and 9c) and electrical (compare Figs. 6 and 9a), and a lower Seebeck coefficient (compare Figs. 6 and 9b). A study of several lanthanide dopants demonstrated that ytterbium additions were most effective for increasing the figure of merit.[137,139] Ytterbium is particularly beneficial in reducing the thermal conductivity[138,140] which is attributed to a decrease in phonon contributions to the thermal conduction.[144] Niobium additions have been shown to lead to an increase in the electrical conductivity and decrease in the thermal conductivity, but also a decrease in the Seebeck coefficient.[145] Similar trends were observed with tantalum additions, but niobium additions resulted in a higher electrical conductivity.[145]

Other lanthanide oxides have been used to dope $CaMnO_3$, the figures of merit for some of which are shown in Fig. 10.[45,139–141,146–148] Lanthanum[149,150] and dysprosium[138,140,151] additions lead to increases in both the electrical conductivity and thermopower of $CaMnO_3$, while praseodymium additions lead to decreases in the thermal conductivity.[152,153] The difference in the properties affected provides opportunities for effective co-doping. For example, the combination of dysprosium, which increases electrical conductivity, with ytterbium, which decreases thermal conductivity, is an effective combination as shown Fig. 10.[140,141] Similarly, the addition of strontium increases the electrical conductivity and

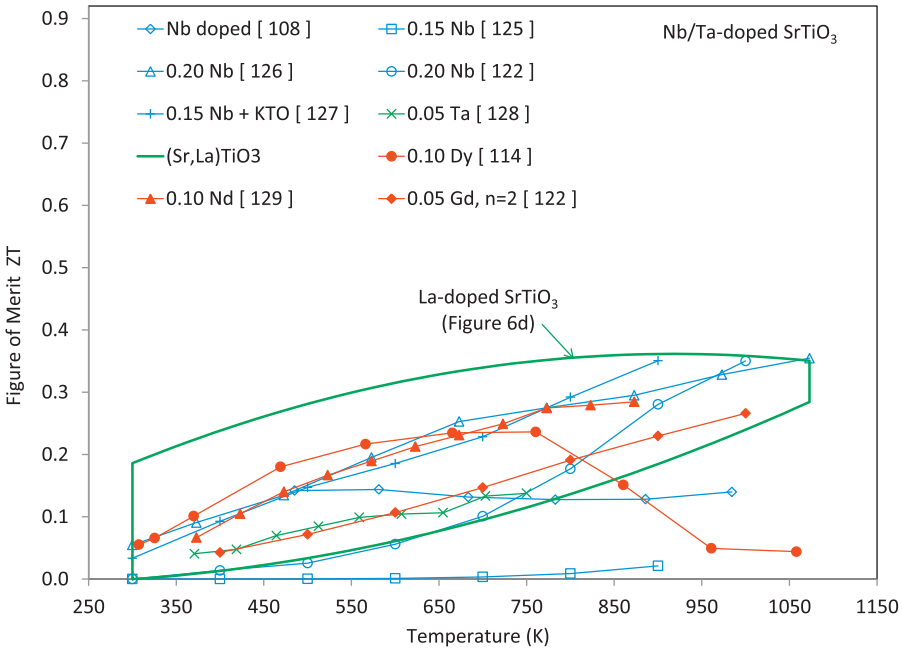

Fig. 8. Electrical conductivity of doped $SrTiO_3$.[108,114,122,123,125–129]

figure of merit of ytterbium doped $CaMnO_3$.[141] However, there are cases where single doping is more effective, such as with dysprosium and niobium.[154] Silver has been shown to increase the Seebeck coefficient[155] while bismuth, either alone[148] or co-doped with vanadium[156] or niobium[157] has been shown to increase the electrical conductivity and the figure of merit.

Ruddlesden–Popper phases based on the calcium–manganese system have been evaluated, but, as discussed above for strontium titanate, do not result in good thermoelectric performance. Fig. 10 shows that the figures of merit for the calcium manganate based Ruddlesden–Popper phases, $Ca_{2.8}La_{0.2}Mn_2O_7$ (labeled R-P 0.2 La) and $Ca_{1.6}Bi_{0.19}MnO_4$ (labeled R-P 0.19 Bi) are quite low.[147,148]

3.3. ZnO

ZnO is another promising thermoelectric material that requires doping for adequate n-type conduction. The thermoelectric properties of aluminum-doped ZnO are summarized in Fig. 11.[82,158–164] The conductivity of doped ZnO can be as high as strontium titanate (compare Figs. 6 and 11a), but ZnO maintains its high conductivity to higher temperatures than strontium titanate. The primary disadvantage of ZnO is that the thermal conductivity is also high. Although ZnO with small amounts of aluminum (*e.g.* 0.25%) have been shown to have low conductivity and low thermopower, larger amounts, on order of 2%, are beneficial.[165] The beneficial effect of aluminum has been attributed to aluminum decreasing the *c*/*a* ratio of the crystal.[166] However, there is also evidence from transmission electron microscopy that second phases are present at the grain boundaries even in samples that appear to be single phase according to X-ray diffraction.[167] Addition evidence for contributions from grain boundaries is in the effect of grain size on properties. For example, the thermal and electrical conductivity of ZnO vary significantly with grain size and the figure of merit has been shown to be better for large grains.[168] These variations may also contribute to the large variations among the results shown in Fig. 11.

Other dopants used for ZnO include nickel, which increases electrical conductivity and thermopower[169] and improves performance as a co-dopant with aluminum.[160] Titanium additions to ZnO also lead to increases in electrical conductivity, but decreases in thermopower.[170] Like nickel, titanium improves performance as a co-dopant with aluminum.[171] Tin[172] and antimony[172,173] used separately, or in combination[172] also increase the conductivity and Seebeck coefficient of ZnO.

4. Implementation in thermoelectric devices

The conventional design for thermoelectric devices consists of a pair of thermoelectric materials – one p-type and one n-type. As shown in Fig. 12a, the two materials are electrically connected at one end, which will be the positive voltage for one material and negative for the other, such that the voltage difference at the other end of the module is the sum of the two thermovoltages. The modules can be connected in series as shown in Fig. 12a to increase the voltage. An alternative design shown in Fig. 12b and referred to as a unileg module uses only one type of thermoelectric material (either p-type or n-type).[174] The voltage generated by each module in the unileg design is smaller, but the metal conductor between the hot and cold ends of the module may occupy less space than the thermoelectric element. The size of the metal conductor must be kept small to minimize the amount of heat transferred between the hot and cold ends of the module. The unileg design requires only one type of thermoelectric material, which may reduce some design restrictions.

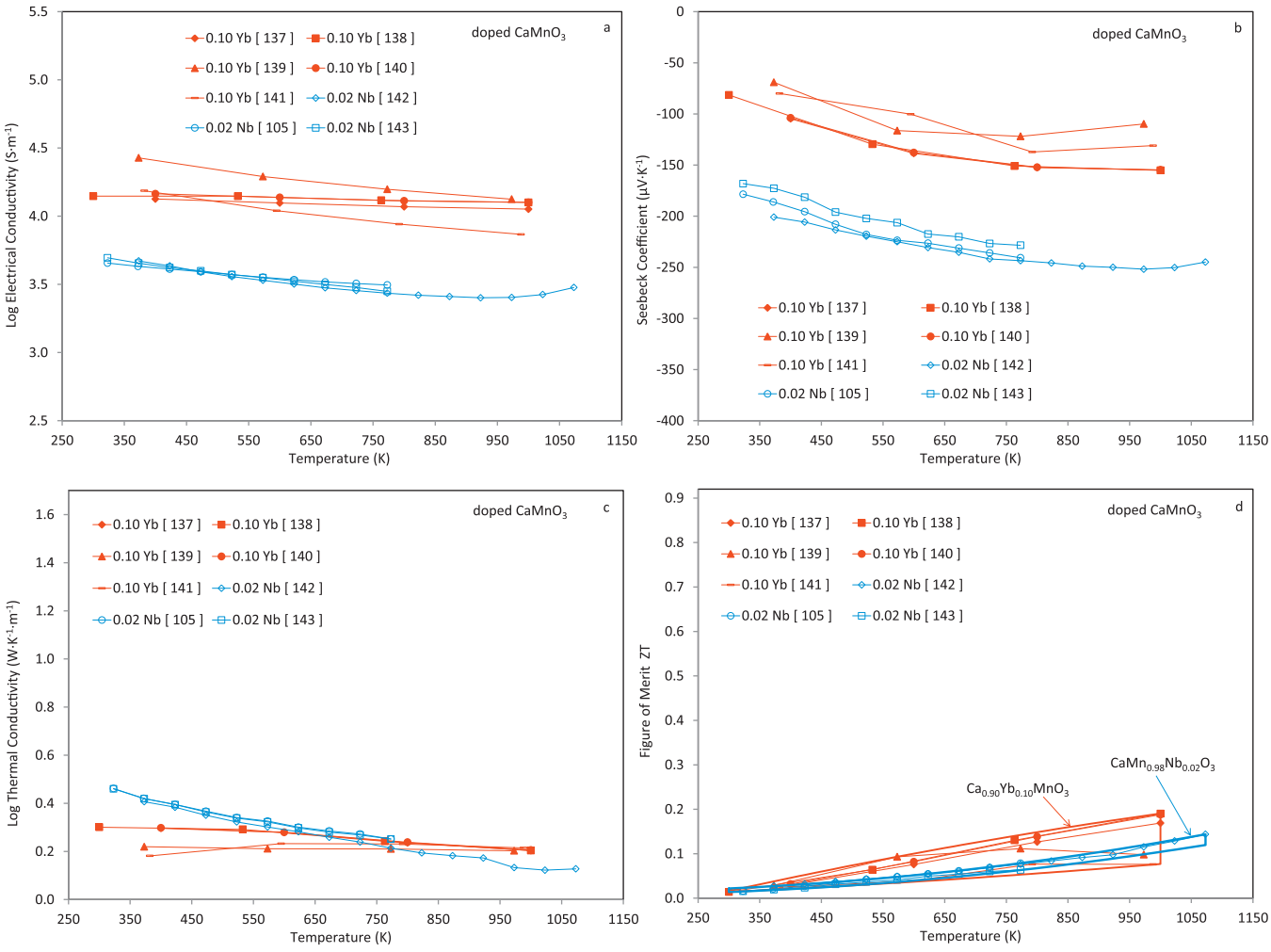

Fig. 9. Electrical conductivity (a), Seebeck coefficient (b), thermal conductivity (c) and figure of merit (*ZT*) (d) for doped $CaMnO_3$.[105,137–143]

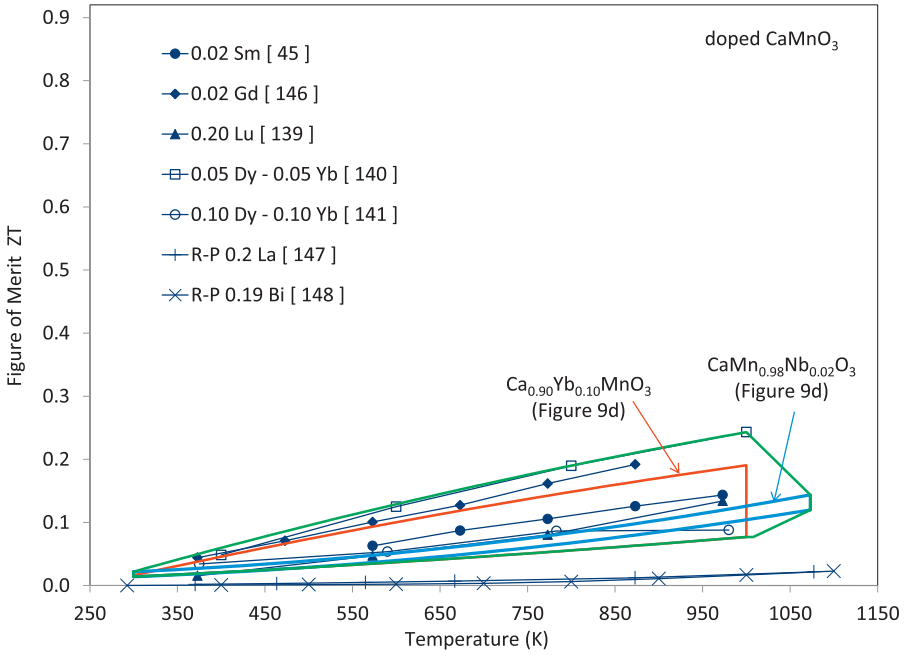

Fig. 10. Figure of merit (*ZT*) for doped $CaMnO_3$.[44,139–141,146–148]

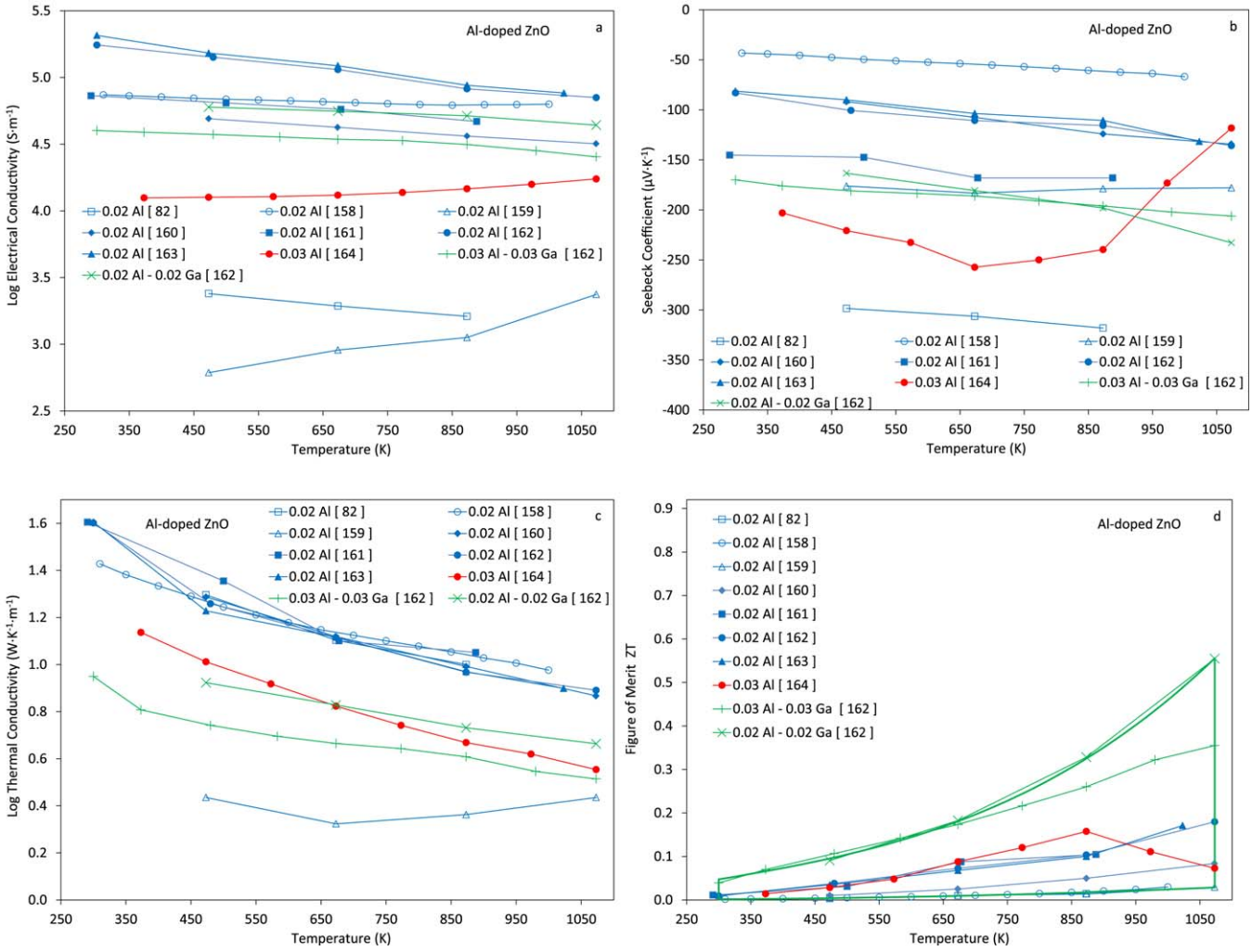

Fig. 11. Electrical conductivity (a), Seebeck coefficient (b), thermal conductivity (c) and figure of merit (*ZT*) (d) for Al-doped ZnO.[82,158–164]. (For interpretation of the references to color in this artwork, the reader is referred to the web version of this article.)

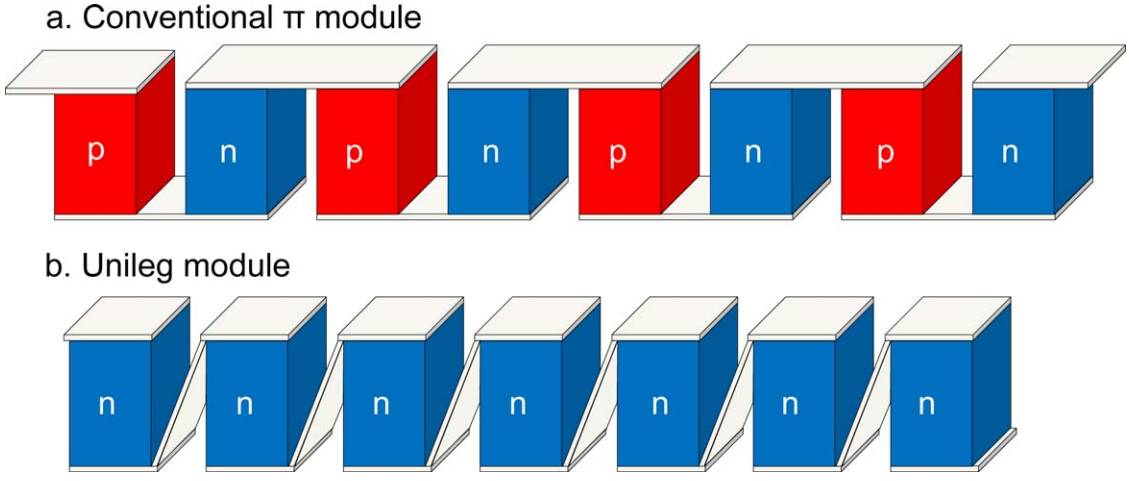

Fig. 12. Conventional (a) and unileg (b) thermoelectric modules.[174]

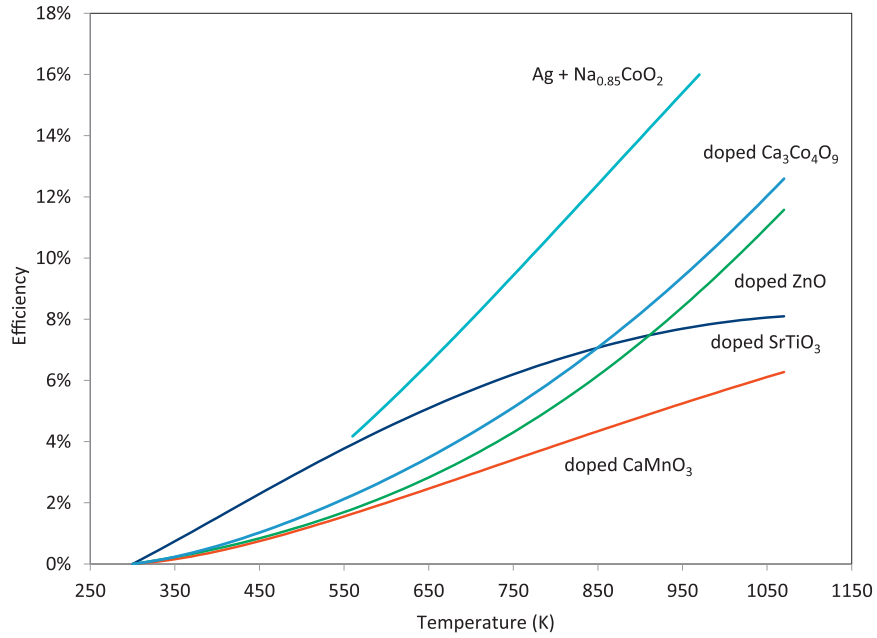

Fig. 13. Maximum theoretical efficiencies for thermoelectric oxides using T_{cold} = 300 K and maximum ZT values from Figs. 3a, 5, 6d, 10, and 11d.

As discussed above, the figure of merit can be used to guide selection of materials. The maximum theoretical efficiency (ε) for conversion of heat transferred from hot temperature, T_H, to cold temperature, T_C, through a material with thermoelectric figure of merit, ZT, is given by Eq. (3).[8]

$$\varepsilon = \left(\frac{T_H - T_C}{T_H}\right) \frac{(\sqrt{1+ZT}-1)}{(\sqrt{1+ZT}-(T_C/T_H))} \quad (3)$$

The maximum values of ZT from Figs. 3a, 5, 6d, 10, and 11d were used to calculate the maximum efficiency from Eq. (3) for a cold temperature of 300 K and are summarized in Fig. 13. Although $Na_{0.85}CoO_2$ has the highest potential efficiency, the poor stability limits its potential application. Among the remaining materials, for a temperature difference of around 500 K, the maximum efficiencies are in the range of 4–6%.

The most common p-type oxides used in thermoelectric devices are based on $Ca_3Co_4O_9$, either undoped[159,175,176] or doped with bismuth ($Ca_{2.7}Bi_{0.3}Co_4O_9$).[124,177,178] The most common thermoelectric n-type oxide is $CaMnO_3$, doped with samarium,[174–176] niobium,[105,143] lanthanum[179] or yttrium.[124] Devices using ZnO doped with aluminum[159] or tin[180] have also been reported. Individual modules typically generate voltages on the order of fractions of a volt and electrical powers in the mW range, but voltages and powers can be increased by combining multiple modules. For example, a 100-pair unit has been shown to produce 12 W at 5 V for a 400 K temperature difference.[124]

The development of reliable and cost-effective thermoelectric devices depends not only on the identification of suitable materials, but also on the associated fabrication processes. General microstructural features, such as porosity and grain size, affect transport of heat and electrical current. As noted above, the properties of ZnO vary significantly with grain size. In addition to these general features, the properties of layered structures are anisotropic, so orientation affects performance. For example, texturing of layered structures, such as $Ca_3Co_4O_9$, has been achieved by pressing,[181–183] rolling[56] or controlled deposition.[184] The processing is further complicated because the devices require small features for fabrication of multi-module assemblies.

5. Conclusions

Both p-type and n-type oxides are available for use in devices for thermoelectric energy conversion. The p-type oxides with the best thermoelectric properties are layered cobaltite compounds. Although Na_xCoO_2 based materials have better thermoelectric performance, $Co_3Co_4O_9$ based materials have better stability and are more widely used. Among the three most widely studied n-type oxides, doped $CoMnO_3$ has lower thermal conductivity, while doped $SrTiO_3$ and doped ZnO have higher electrical conductivity. Although the thermoelectric properties of these oxides are not as good as those of the some non-oxide compounds, such as tellurides and antimonides, they have better stability and thus may be suitable for high temperature applications. Additional improvements in materials properties and the associated fabrication processes are needed for the development of economically feasible devices.

References

1. Bennett GL. Space nuclear power: opening the final frontier. In: *Proc 4th Int Energy Conversion Engineering Conf Exhibit (IECEC), AIAA, 4191*. 2006. p. 1–17.
2. Sneve MK. Remote control. *IAEA Bull* 2006;**48**:42–7.
3. Yang J, Stabler FR. Automotive applications of thermoelectric materials. *J Electron Mater* 2009;**38**:1245–51.
4. Korzhuev MA, Katin IV. On the placement of thermoelectric generators in automobiles. *J Electron Mater* 2010;**39**:1390–4.

5. Kim S-K, Won B-C, Rhi S-H, Kim S-H, Yoo J-H, Jang J-C. Thermoelectric power generation system for future hybrid vehicles using hot exhaust gas. *J Electron Mater* 2011;**40**:778–83.
6. Patyk A. Thermoelectrics: impacts on the environment and sustainability. *J Electron Mater* 2010;**39**:2023–8.
7. Anatychuk LI, Rozver Yu, Velichuk DD. Thermoelectric generator for a stationary diesel plant. *J Electron Mater* 2011;**40**:1206–8.
8. Nemir D, Beck J. On the significance of the thermoelectric figure of merit Z. *J Electron Mater* 2010;**39**:1897–901.
9. Sebald G, Guyomar D, Agbossou A. On thermoelectric and pyroelectric energy harvesting. *Smart Mater Struct* 2009;**18**:125006-1–7.
10. Doumerc JP, Blangero M, Pollet M, Carlier D, Darriet J, Berthelot R, et al. Transition-metal oxides for thermoelectric generation. *J Electron Mater* 2009;**38**:1078–82.
11. Böttner H. Thermoelectrics for high temperatures – a survey of state of the art. *Mater Res Soc Symp Proc* 2009;**1166**:N01.
12. Toberer ES, May AF, Snyder GJ. Zintl chemistry for designing high efficiency thermoelectric materials. *Chem Mater* 2010;**22**:624–34.
13. Ohta H, Sugiura K, Koumoto K. Recent progress in oxide thermoelectric materials: p-type $Ca_3Co_4O_9$ and n-Type $SrTiO_3$. *Inorg Chem* 2008;**47**:8429–36.
14. Kanatzidis MG. Nanostructured thermoelectrics: the new paradigm? *Chem Mater* 2010;**22**:648–59.
15. Salzgeber K, Prenninger P, Grytsiv A, Rogl P, Bauer E. Skutterudites: thermoelectric materials for automotive applications? *J Electron Mater* 2010;**39**:2028–74.
16. Li Q, Lin Z, Zhou J. Thermoelectric materials with potential high power factors for electricity generation. *J Electron Mater* 2009;**38**:1268–72.
17. Koshibae W, Tsutsui K, Maekawa S. Thermopower in cobalt oxides. *Phys Rev B* 2000;**62**:6869–72.
18. Karppinen M, Fjellvåg H, Konno T, Morita Y, Motohashi T, Yamauchi H. Evidence for oxygen vacancies in misfit-layered calcium cobalt oxide $[CoCa_2O_3]_qCoO_2$. *Chem Mater* 2004;**16**:2790–3.
19. Matsubara I, Funahashi R, Shikano M, Sasaki K, Enomoto H. Cation substituted $(Ca_2CoO_3)_xCoO_2$ films and their thermoelectric properties. *Appl Phys Lett* 2002;**80**:4729–31.
20. Ling CD, Aivazian K, Schmid S, Jensen P. Structural investigation of oxygen non-stoichiometry and cation doping in misfit-layered thermoelectric $(Ca_2CoO_{3-x})(CoO_2)_\delta$ $\delta \sim 1.61$. *J Solid State Chem* 2007;**180**:1446–55.
21. Fukutomi H, Konno Y, Okayasu K, Hasegawa M, Nakatsugawa H. Texture development of $Ca_3Co_4O_9$ thermoelectric oxide by high temperature plastic deformation and its contribution to the improvement in electric conductivity. *Mater Sci Eng A* 2009;**527**:61–4.
22. Tyson TA, Chen Z, Jie Q, Li Q, Tu JJ. Local structure of thermoelectric $Ca_3Co_4O_9$. *Phys Rev B* 2009;**79**:024109-1–7.
23. Morita Y, Poulsen J, Sakai K, Motohashi T, Fujii T, Terasaki I, et al. Oxygen nonstoichiometry and cobalt valence in misfit-layered cobalt oxides. *J Solid State Chem* 2004;**177**:3149–55.
24. Oide Y, Miyazaki Y, Huang XY, Kajitani T. Thermogravimetric study and high-temperature thermoelectric properties of $[Ca_2(Co_{1-x}A_x)O_3]_{0.62}CoO_2$. In: *Proc 2006 Int Conf Thermoelectrics, IEEE*. 2006. p. 402–5.
25. Shamoto S-I, Hasegawa Y, Kajitani T. Two-dimensional sodium fluctuation at high temperatures in high-temperature thermoelectric material γ-$Na_{0.7}CoO_2$. *Jpn J Appl Phys* 2006;**45**:6395–7.
26. Takahashi Y, Akimoto J, Kijima N, Gotoh Y. Structure and electron density analysis of $Na_{0.74}CoO_2$ by single-crystal X-ray diffraction. *Solid State Ionics* 2004;**172**:505–8.
27. Li N, Jiang Y, Li G, Wang C, Shi J, Yu D. Self-ignition route to Ag-doped $Na_{1.7}Co_2O_4$ and its thermoelectric properties. *J Alloys Compd* 2009;**467**:444–9.
28. Dutta D, Battogtokh J, McKewon D, Vidensky I, Dutta N, Pegg IL. Thermoelectric properties of $NaCo_{2-x}Fe_xO_y$. *J Electron Mater* 2007;**36**:746–52.
29. Sun T, Hng HH, Yan Q, Ma J. Effects of pulsed laser deposition conditions on the microstructure of $Ca_3Co_4O_9$ thin films. *J Electron Mater* 2010;**39**:1611–5.
30. Tahashi M, Tanimoto T, Goto H, Takahashi M, Ido T. Sintering temperature dependence of thermoelectric performance and crystal phase of calcium cobalt oxides. *J Am Ceram Soc* 2010;**93**:3046–8.
31. Lu QM, Zhang JX, Zhang QY, Liu YQ, Liu DM. Improved thermoelectric properties of $Ca_{3-x}Ba_xCo_4O_9$ ($x = 0$–0.4) bulks by sol–gel and SPS method. *Proc 2006 Int Conf Thermoelectrics, IEEE* 2006:66–9.
32. Katsuyama S, Takiguchi Y, Ito M. Synthesis of $Ca_3Co_4O_9$ ceramics by polymerized complex and hydrothermal hot-pressing processes and investigation of its thermoelectric properties. *Proc 2006 Int Conf Thermoelectrics, IEEE* 2006:103–7.
33. Kwon O-J, Jo W, Ko K-E, Kim J-Y, Bae S-H, Koo H, et al. Thermoelectric properties and texture evaluation of $Ca_3Co_4O_9$ prepared by a cost-effective multisheetcofiring technique. *J Mater Sci* 2011;**46**:2887–94.
34. Wang D, Chen L, Yao Q, Li J. High-temperature thermoelectric properties of $Ca_3Co_4O_{9+\delta}$ with Eu substitution. *Solid State Commun* 2004;**129**:615–8.
35. Wang D, Chen L, Wang Q, Li J. Fabrication and thermoelectric properties of $Ca_{3-x}Dy_xCo_4O_{9+\delta}$ system. *J Alloys Compd* 2004;**376**:58–61.
36. Yin T, Liu D, Ou Y, Ma F, Xie S, Li JF, et al. Nanocrystalline thermoelectric $Ca_3Co_4O_9$ ceramics by sol–gel based electrospinning and spark plasma sintering. *J Phys Chem C* 2010;**114**:10061–5.
37. Nong NV, Liu C-J, Ohtaki M. Improvement on the high temperature thermoelectric performance of Ga-doped misfit-layered $Ca_3Co_{4-x}Ga_xO_{9+\delta}$ ($x = 0$, 0.05, 0.1, and 0.2). *J Alloys Compd* 2010;**491**:53–6.
38. Nong NV, Yanagiya S, Monica S, Pryds N, Ohtaki M. High-temperature thermoelectric and microstructural characteristics of cobalt-based oxides with Ga substituted on the Co-site. *J Electron Mater* 2011;**40**:716–22.
39. Nong NV, Pryds N, Linderoth S, Ohtaki M. Enhancement of the thermoelectric performance of p-type layered oxide $Ca_3Co_4O_{9+\delta}$ through heavy doping and metallic nanoinclusions. *Adv Mater* 2011;**23**:2484–90.
40. Nong NV, Liu C-J, Ohtaki M. High-temperature thermoelectric properties of late rare earth-doped $Ca_3Co_4O_9$. *J Alloys Compd* 2011;**509**:977–81.
41. Zhang FP, Lu QM, Zhang JX. Synthesis and high temperature thermoelectric properties of $Ba_xAg_yCa_{3-x-y}Co_4O_9$ compounds. *J Alloys Compd* 2009;**484**:550–4.
42. Liu Y, Lin Y, Jiang L, Nan C-W, Shen Z. Thermoelectric properties of Bi^{3+} substituted Co-based misfit-layered oxides. *J Electroceram* 2008;**21**:748–51.
43. Pei J, Chen G, Zhou N, Lu DQ, Xiao F. High temperature transport and thermoelectric properties of $Ca_{3-x}Er_xCo_4O_{9+\delta}$. *Physica B* 2011;**406**:571–4.
44. Lim C-H, Choi S-M, Seo W-S. High-temperature thermoelectric properties of the $Ca_{3-x}K_xCo_4O_9$ ($0 \le x \le 0.3$) system. *J Korean Phys Soc* 2010;**57**:1054–8.
45. Su H, Jiang Y, Lan X, Liu X, Zhong H, Yu D. $Ca_{3-x}Bi_xCo_4O_9$ and $Ca_{1-y}Sm_yMnO_3$ thermoelectric materials and their power-generation devices. *Phys Status Solidi A* 2011;**208**:147–55.
46. Wang Y, Sui Y, Wang X, Su W, Liu X. Enhanced high temperature thermoelectric characteristics of transition metals doped $Ca_3Co_4O_{9+\delta}$ by cold high-pressure fabrication. *J Appl Phys* 2010;**107**:033708-1–9.
47. Xu L, Li F, Wang Y. High-temperature transport and thermoelectric properties of $Ca_3Co_{4-x}Ti_xO_9$. *J Alloys Compd* 2010;**501**:115–9.
48. Delorme F, Martin CF, Marudhachalam P, Ovono DO, Guzman G. Effect of Ca substitution by Sr on the thermoelectric properties of $Ca_3Co_4O_9$ ceramics. *J Alloys Compd* 2011;**509**:2311–5.
49. Liu HQ, Song Y, Zhang SN, Zhao XB, Wang FP. Thermoelectric properties of $Ca_{3-x}Y_xCo_4O_{9+\delta}$ ceramics. *J Phys Chem Solids* 2009;**70**:600–3.
50. Li S, Funahashi R, Matsubara I, Ueno K, Sodeoka S, Yamada H. Synthesis and thermoelectric properties of the new oxide materials $Ca_{3-x}Bi_xCo_4O_{9+\delta}$ ($0.0 < x < 0.75$). *Chem Mater* 2000;**12**:2424–7.
51. Song Y, Sun Q, Zhao L, Wang F, Jiang Z. Synthesis and thermoelectric power factor of $(Ca_{0.95}Bi_{0.05})_3Co_4O_9$/Ag composites. *Mater Chem Phys* 2009;**113**:645–9.
52. Sun T, Hng HH, Yan QY, Ma J. Enhanced high temperature thermoelectric properties of Bi-doped *c*-axis oriented $Ca_3Co_4O_9$ thin films by pulsed laser deposition. *J Appl Phys* 2010;**108**:083709-1–5.

53. Hao H, Zhao L, Hu X. Microstructure and thermoelectric properties of Bi- and Cu-substituted $Ca_3Co_4O_9$ oxides. *J Mater Sci Technol* 2009;**25**:105–8.
54. Xu G, Funahashi R, Shikano M, Matsubara I, Zhou Y. Thermoelectric properties of the Bi- and Na-substituted $Ca_3Co_4O_9$ system. *Appl Phys Lett* 2002;**80**:3660–762.
55. Lan J, Lin YH, Li G-J, Xu S, Liu Y, Nan C-W, et al. High-temperature electrical transport behaviors of the layered $Ca_2Co_2O_5$-based ceramics. *Appl Phys Lett* 2010;**96**:192104-1–3.
56. Park JW, Kwak DH, Yoon SH, Choi SC. Thermoelectric properties of highly oriented $Ca_{2.7}Bi_{0.3}Co_4O_9$ fabricated by rolling processes. *J Ceram Soc Jpn* 2009;**117**:643–6.
57. Wang Y, Sui Y, Cheng J, Wang X, Su W. Comparison of the high temperature thermoelectric properties for Ag-doped and Ag-added $Ca_3Co_4O_9$. *J Alloys Compd* 2009;**477**:817–21.
58. Wang Y, Sui Y, Cheng J, Wang X, Miao J, Liu Z, et al. High temperature transport and thermoelectric properties of Ag-substituted $Ca_3Co_4O_{9+\delta}$ system. *J Alloys Compd* 2008;**48**:1–5.
59. Zhang FP, Lu QM, Zhang JX, Zhang X. Texture and high temperature transport properties of $Ag_xCa_{3-x}Co_4O_9$ ($0 \le x \le 0.6$) compounds. *J Alloys Compd* 2009;**477**:536–43.
60. Wang Y, Sui Y, Cheng J, Wang X, Su W. Efficient room temperature thermoelectric characteristics of $Ca_{3-x}Ag_xCo_4O_{9+\delta}/Ag_y$ composites. *J Phys D: Appl Phys* 2008;**41**:045406-1–7.
61. Zhang FP, Lu QM, Zhang JX. Modified texture and high temperature transport properties of doubly substituted $Ba_xAg_yCa_{2.8}Co_4O_9$ thermoelectric oxide. *Physica B* 2009;**404**:2142–5.
62. Mikami M, Ando N, Funahashi R. The effect of Ag addition on electrical properties of the thermoelectric compound $Ca_3Co_4O_9$. *J Solid State Chem* 2005;**178**:2186–90.
63. Xiang P-H, Kinemuchi Y, Kaga H, Watari K. Fabrication and thermoelectric properties of $Ca_3Co_4O_9$/Ag composites. *J Alloys Compd* 2008;**454**:364–9.
64. Rivas-Murias B, Muguerra H, Traianidis M, Henrist C, Vertruyen B, Cloots R. Enhancement of the power factor of $[Bi_{1.68}Ca_2O_4]^{RS}[CoO_2]_{1.69}$ – Ag composites prepared by the spray-drying method. *Solid State Sci* 2010;**12**:1490–5.
65. Song Y, Nan C-W. High temperature transport properties of Ag-added $(Ca_{0.975}La_{0.025})_3Co_4O_9$ ceramics. *Physica B* 2011;**406**:2919–23.
66. Yao Q, Wang DL, Chen LD, Shi X, Zhou M. Effects of partial substitution of transition metals for cobalt on the high-temperature thermoelectric properties of $Ca_3Co_4O_{9+\delta}$. *J Appl Phys* 2005;**9**:103905-1–5.
67. Mikami M, Funahashi R. The effect of element substitution on high-temperature thermoelectric properties of $Ca_3Co_2O_6$ compounds. *J Solid State Chem* 2005;**178**:1670–4.
68. Park K, Kim KK, Kim SJ, Lee N, Yang B. High-temperature thermoelectric properties of Cu-doped $Ca_{3-x}Cu_xCo_4O_9$ ($0 \le x \le 0.4$). *J Korean Phys Soc* 2006;**49**:1553–7.
69. Takami T, Ikuta H. Magnetic and thermoelectric properties of quasi-one-dimensional oxides $A_{n+2}CoB_nO_{3n+3}$ (A = Ca, Sr, B = Co, Rh, Ir; n = 1–3). *J Appl Phys* 2008;**103**, 07B701-1–07B701-3.
70. Matsubara I, Funahashi R, Takeuchi T, Sodeoka S. Thermoelectric properties of spark plasma sintered $Ca_{2.75}Gd_{0.25}Co_4O_9$ ceramics. *J Appl Phys* 2001;**90**:462–5.
71. Pei J, Chen G, Lu DQ, Liu PS, Zhou N. Synthesis and high temperature thermoelectric properties of $Ca_{3.0-x-y}Nd_xNa_yCo_4O_{9+\delta}$. *Solid State Commun* 2008;**146**:283–6.
72. Nan J, Wu J, Deng Y, Nan CW. Synthesis and thermoelectric properties of $(Na_xCa_{1-x})_3Co_4O_9$ ceramics. *J Eur Ceram Soc* 2003;**23**:859–63.
73. Sotelo A, RasekhSh, Madre MA, Guilmeau E, Marinel S, Diez JC. Solution-based synthesis routes to thermoelectric $Bi_2Ca_2Co_{1.7}O_x$. *J Eur Ceram Soc* 2011;**31**:1763–9.
74. Shen JJ, Liu XX, Zhu TJ, Zhao XB. Improved thermoelectric properties of La-doped $Bi_2Sr_2Co_2O_9$-layered misfit oxides. *J Mater Sci* 2009;**44**:1889–93.
75. Lin Y-H, Nan C-W, Liu Y, Li J, Mizokawa T, Shen Z. High-temperature electrical transport and thermoelectric power of partially substituted $Ca_3Co_4O_9$-based ceramics. *J Am Ceram Soc* 2007;**90**:132–6.
76. Lin YH, Lan J, Shen Z, Liu Y, Nan C-W, Li J-F. High-temperature electrical transport behaviors in textured $Ca_3Co_4O_9$-based polycrystalline ceramics. *Appl Phys Lett* 2009;**94**:072107-1–172107-3.
77. Prevel M, Reddy ES, Perez O, Kobayashi W, Terasaki I, Goupil C, et al. Thermoelectric properties of sintered and textured Nd-substituted $Ca_3Co_4O_9$ ceramics. *Jpn J Appl Phys* 2007;**46**:6533–8.
78. Xu J, Wei C, Jia K. Thermoelectric performance of textured $Ca_{3-x}Yb_xCo_4O_{9-\delta}$ ceramics. *J Alloys Compd* 2010;**500**:227–30.
79. Nong NV, Ohtaki M. Thermoelectric properties and local electronic structure of rare earth-doped $Ca_3Co_2O_6$. In: *Proc 2006 Int Conf Thermoelectrics, IEEE*. 2006. p. 62–5.
80. Liu PS, Chen G, Pei J, Cui Y, Lu DQ, Zhou N, et al. Preparation and characterization of the new oxides $Ca_{2-x}Na_xCo_2O_5$. *Physica B* 2008;**403**:1808–12.
81. Senthilkumar M, Vijayaraghavan R. High-temperature resistivity and thermoelectric properties of coupled substituted $Ca_3Co_2O_6$. *Sci Technol Adv Mater* 2009;**10**:015007-1–5.
82. Fujishiro Y, Miyata M, Awano M, Maeda K. Characterization of thermoelectric metal oxide elements prepared by the pulse electric-current sintering method. *J Am Ceram Soc* 2004;**87**:1890–4.
83. Nagira T, Ito M, Katsuyama S, Majima K, Nagai H. Thermoelectric properties of $(Na_{1-y}M_y)_xCo_2O_4$ (M = K, Sr, Y, Nd, Sm and Yb; y = 0.01–0.35). *J Alloys Compd* 2003;**348**:263–9.
84. Wang L, Wang M, Zhao D. Thermoelectric properties of *c*-axis oriented Ni-substituted $NaCoO_2$ thermoelectric oxide by the citric acid complex method. *J Alloys Compd* 2009;**471**:519–23.
85. Tsai PH, Norby T, Tan TT, Donelson R, Chen ZD, Li S. Correlation of oxygen vacancy concentration and thermoelectric properties in $Na_{0.73}CoO_{2-\delta}$. *Appl Phys Lett* 2010;**96**:141905-1–3.
86. Ito M, Furumoto D. Microstructure and thermoelectric properties of $Na_xCo_2O_4$/Ag composite synthesized by the polymerized complex method. *J Alloys Compd* 2008;**450**:517–20.
87. Liu P, Chen G, Cui Y, Zhang H, Xiao F, Wang L, et al. High temperature electrical conductivity and thermoelectric power of Na_xCoO_2. *Solid State Ionics* 2008;**179**:2308–12.
88. Singh DJ, Kasinathan D. Thermoelectric properties of Na_xCoO_2 and prospects for other oxide thermoelectrics. *J Electron Mater* 2007;**36**:736–9.
89. Seetawan T, Amornkitbamrung V, Burinprakhon T, Maensiri S, Kurosaki K, Muta H, et al. Thermoelectric power and electrical resistivity of Ag-doped $Na_{1.5}Co_2O_4$. *J Alloys Compd* 2006;**407**:314–7.
90. Seetawan T, Amornkitbamrung V, Burinprakhon T, Maensiri S, Kurosaki K, Muta H, et al. Thermoelectric properties of $Na_xCo_2O_4$/Ag composites. *J Alloys Compd* 2006;**414**:293–7.
91. Ito M, Furumoto D. Effects of noble metal addition on microstructure and thermoelectric properties of $Na_xCo_2O_4$. *J Alloys Compd* 2008;**450**:394–498.
92. Park K, Jang KU, Kwon H-C, Kim J-G, Cho W-S. Influence of partial substitution of Cu for Co on the thermoelectric properties of $NaCo_2O_4$. *J Alloys Compd* 2006;**419**:213–9.
93. Park K, Ko KY, Kim J-G, Cho W-S. Microstructure and high-temperature thermoelectric properties of CuO and NiO co-substituted $NaCo_2O_4$. *Mater Sci Eng B* 2006;**129**:200–6.
94. Park K, Lee JH. Enhanced thermoelectric properties of $NaCo_2O_4$ by adding ZnO. *Mater Lett* 2008;**62**:2366–8.
95. Tsai PH, Zhang TS, Donelson R, Tan TT, Li S. Power factor enhancement in Zn-doped $Na_{0.8}CoO_2$. *J Alloys Compd* 2011;**509**:5183–6.
96. Park K, Jang KU. Improvement in high-temperature thermoelectric properties of $NaCo_2O_4$ through partial substitution of Ni for Co. *Mater Lett* 2006;**60**:1106–10.
97. Ito M, Nagira T, Hara S. Thermoelectric properties of $Na_xCo_2O_4$ with rare-earth metals doping prepared by polymerized complex method. *J Alloys Compd* 2006;**408–412**:1217–21.
98. Kenfaui D, Chateigner D, Gomina M, Noudem JG. Anisotropy of the mechanical and thermoelectric properties of hot-pressed single-layer and multilayer thick $Ca_3Co_4O_9$ ceramics. *Int J Appl Ceram Technol* 2011;**8**:214–26.

99. Kenfaui D, Bonnefont G, Chateigner D, Fantozzi G, Gomina M, Noudem JG. $Ca_3Co_4O_9$ ceramics consolidated by SPS process: optimisation of mechanical and thermoelectric properties. *Mater Res Bull* 2010;**45**:1240–9.
100. Zhou AJ, Zhu TJ, Zhao XB, Chen HY, Müller E. Fabrication and thermoelectric properties of perovskite-type oxide $La_{1-x}Sr_xCoO_3$ ($x = 0$, 0. 1). *J Alloys Compd* 2008;**449**:105–8.
101. Robert R, Aguirre MH, Hug P, Reller A, Weidenkaff A. High-temperature thermoelectric properties of Ln(Co, Ni)O_3 (Ln = La, Pr, Nd, Sm, Gd and Dy) compounds. *Acta Mater* 2007;**55**:4965–72.
102. Li F, Li J-F. Effect of Ni substitution on electrical and thermoelectric properties of $LaCoO_3$ ceramics. *Ceram Int* 2011;**37**:105–10.
103. Li J, Smith AE, Kwong K-S, Powell C, Sleight AW, Subramanian MA. Lattice crossover and mixed valency in the $LaCo_{1-x}Rh_xO_3$ solid solution. *J Solid State Chem* 2010;**183**:1388–93.
104. Kwong K-S, Smith AE, Subramanian MA. The effect of Rh and Sr substitution on the thermoelectric performance of $LaCoO_3$. *Mater Res Soc Symp Proc* 2010;**1267**:DD11–2.
105. Tomeš P, Trottman M, Suter C, Aguirre MH, Steinfeld A, Haueter P, et al. Thermoelectric oxide modules (TOMs) for the direct conversion of simulated solar radiation into electrical energy. *Materials* 2010;**3**:2801–14.
106. Liu C, Ren F, Wang H, Case E, Morelli D. Solid-state synthesis and some properties of magnesium-doped copper aluminum oxides. *Mater Res Soc Symp Proc* 2010;**1218**:Z01–5.
107. Yanagiya S-I, Nong NV, Xu J, Pryds N. The effect of (Ag, Ni, Zn)-addition on the thermoelectric properties of copper aluminate. *Materials* 2010;**3**:318–28.
108. Ohta S, Nomura T, Ohta H, Koumoto K. High-temperature carrier transport and thermoelectric properties of heavily La- or Nb-doped $SrTiO_3$ single crystals. *J Appl Phys* 2005;**97**:034106-1–4.
109. Muta H, Kurosaki K, Yamanaka S. Thermoelectric properties of reduced and La-doped single-crystalline $SrTiO_3$. *J Alloys Compd* 2005;**392**:306–9.
110. Liu J, Wang CL, Su WB, Wang HC, Zheng P, Li JC, et al. Enhancement of thermoelectric efficiency in oxygen-deficient $Sr_{1-x}La_xTiO_{3-\delta}$ ceramics. *Appl Phys Lett* 2009;**95**:162110-1–3.
111. Ravichandran J, Siemons W, Oh D-W, Kardel JT, Chari A, Heijmerikx H, et al. High-temperature thermoelectric response of double-doped $SrTiO_3$ epitaxial films. *Phys Rev B* 2010;**82**:155126-5–65126-1.
112. Kikuchi A, Okinaka N, Akiyama T. A large thermoelectric figure of merit of La-doped $SrTiO_3$ prepared by combustion synthesis with post-spark plasma sintering. *Scripta Mater* 2010;**63**:407–10.
113. Shang P-P, Zhang B-P, Li J-F, Ma N. Effect of sintering temperature on thermoelectric properties of La-doped $SrTiO_3$ ceramics prepared by sol–gel process and spark plasma sintering. *Solid State Sci* 2010;**12**:1341–6.
114. Muta H, Kurosaki K, Yamanaka S. Thermoelectric properties of rare earth doped $SrTiO_3$. *J Alloys Compd* 2003;**350**:292–5.
115. Wang HC, Wang CL, Su WB, Liu J, Peng H, Sun Y, et al. Synthesis and thermoelectric performance of Ta doped $Sr_{0.9}La_{0.1}TiO_3$ ceramics. *Ceram Int* 2011;**35**:2609–13.
116. Muta H, Kurosaki K, Yamanaka S. Thermoelectric properties of doped $BaTiO_3$–$SrTiO_3$ solid solution. *J Alloys Compd* 2004;**368**:22–4.
117. Shang P-P, Zhang B-P, Liu Y, Li J-F, Zhu H-M. Preparation and thermoelectric properties of La-doped $SrTiO_3$ ceramics. *J Electron Mater* 2011;**40**:926–31.
118. Okinaka N, Zhang L, Akiyama T. Thermoelectric properties of rare earth-doped $SrTiO_3$ using combination of combustion synthesis (CS) and spark plasma sintering (SPS). *ISIJ Int* 2010;**50**:1300–4.
119. Kinaci A, Sevik C, Çağın T. Electronic transport properties of $SrTiO_3$ and its alloys: $Sr_{1-x}La_xTiO_3$ and $SrTi_{1-x}M_xO_3$ (M = Nb, Ta). *Phys Rev B* 2010;**82**:155114-1–8.
120. Wang YF, Lee KH, Ohta H, Koumoto K. Fabrication and thermoelectric properties of heavily rare-earth metal-doped $SrO(SrTiO_3)_n$ ($n = 1$, 2) ceramics. *Ceram Int* 2008;**34**:849–52.
121. Wang YF, Lee KH, Ohta H, Koumoto K. Thermoelectric properties and their relation to crystal structure of rare earth (RE = La, Nd, Sm and Gd)-doped $SrO(SrTiO_3)_2$ Ruddelseden–Popper phase. *Proc 2006 Int Conf Thermoelectrics, IEEE* 2006:157–60.
122. Wang YF, Lee KH, Ohta H, Koumoto K. Thermoelectric properties of electron doped $SrO(SrTiO_3)_n$ ($n = 1$, 2) ceramics. *J Appl Phys* 2009;**105**:103701-1–6.
123. Wang Y, Lee KH, Hyuga H, Kita H, Ohta H, Koumoto K. Enhancement of thermoelectric performance in rare earth-doped $Sr_3Ti_2O_7$ by symmetry restoration of TiO_6 octahedra. *J Electroceram* 2010;**24**:76–82.
124. Koumoto K, Wang Y, Zhang R, Kosuga A, Funahashi R. Oxide thermoelectric materials: a nanostructuring approach. *Annu Rev Mater Res* 2010;**40**:363–94.
125. Wang N, Han L, He H, Ba Y, Koumoto K. Effects of mesoporous silica addition on thermoelectric properties of Nb-doped $SrTiO_3$. *J Alloys Compd* 2010;**497**:308–11.
126. Kato K, Yamamoto M, Ohta S, Muta H, Kurosaki K, Yamanaka S, et al. The effect of Eu substitution on thermoelectric properties of $SrTi_{0.8}Nb_{0.2}O_3$. *J Appl Phys* 2007;**102**:116107-1–3.
127. Wang N, He H, Ba Y, Wan C, Koumoto K. Thermoelectric properties of Nb-doped $SrTiO_3$ ceramics enhanced by potassium titanate nanowires addition. *J Ceram Soc Jpn* 2010;**118**:1098–101.
128. Cui Y, Salvador JR, Yang J, Wang H, Amow G, Kleinke H. Thermoelectric properties of heavily doped n-type $SrTiO_3$ bulk materials. *J Electron Mater* 2009;**38**:1002–7.
129. Liu J, Wang CL, Su WB, Wang HC, Li JC, Zhang JL, et al. Thermoelectric properties of $Sr_{1-x}Nd_xTiO_3$ ceramics. *J Alloys Compd* 2010;**492**:L54–6.
130. Wang HC, Wang CL, Su WB, Liu J, Zhao Y, Peng H, et al. Enhancement of thermoelectric figure of merit by doping Dy in $La_{0.1}Sr_{0.9}TiO_3$ ceramic. *Mater Res Bull* 2010;**45**:809–12.
131. Wang HC, Wang CL, Su WB, Liu J, Sun Y, Peng H, et al. Doping effect of La and Dy on the thermoelectric properties of $SrTiO_3$. *J Am Ceram Soc* 2011;**94**:838–42.
132. Ito M, Matsuda T. Thermoelectric properties of non-doped and Y-doped $SrTiO_3$ polycrystals synthesized by polymerized complex process and hot pressing. *J Alloys Compd* 2009;**477**:473–7.
133. Obara H, Yamamoto A, Lee C-H, Kobayashi K, Matsumoto A, Funahashi R. Thermoelectric properties of Y-doped polycrystalline $SrTiO_3$. *Jpn J Appl Phys* 2004;**43**:L540–2.
134. Frederikse HPR, Thurber WR, Hosler WR. Electronic transport in strontium titanate. *Phys Rev* 1964;**134**:A442–5.
135. Lee KH, Ishizaki A, Kim SW, Ohta H, Koumoto K. Preparation and thermoelectric properties of heavily Nb-doped SrO $(SrTiO_3)_1$ epitaxial films. *J Appl Phys* 2007;**102**:033702-1–4.
136. Ohta S, Nomura T, Ohta H, Hirano M, Hosono H, Koumoto K. Large thermoelectric performance of heavily Nb-doped $SrTiO_3$ epitaxial film at high temperature. *Appl Phys Lett* 2005;**87**:092108-1–3.
137. Wang Y, Sui Y, Fan H, Wang X, Su Y, Su W, et al. High temperature thermoelectric response of electron-doped $CaMnO_3$. *Chem Mater* 2009;**21**:4653–60.
138. Wang Y, Sui Y, Su W. High temperature thermoelectric characteristics of $Ca_{0.9}R_{0.1}MnO_3$ (R = La, Pr, . . ., Yb). *J Appl Phys* 2008;**104**:093703-1–7.
139. Funahashi R, Kosuga A, Miyasou N, Takeuchi E, Urata S, Lee K, et al. Thermoelectric properties of $CaMnO_3$ system. *Proc 2006 Int Conf Thermoelectrics, IEEE* 2006:124–8.
140. Wang Y, Sui Y, Wang X, Su W. Enhancement of thermoelectric efficiency in (Ca,Dy)MnO_3–(Ca,Yb)MnO_3 solid solutions. *Appl Phys Lett* 2010;**97**:052109-1–3.
141. Kosuga A, Isse Y, Wang Y, Koumoto K, Funahashi R. High-temperature thermoelectric properties of $Ca_{0.9-x}Sr_xYb_{0.1}MnO_{3-\delta}$ ($0 \le x \le 0.2$). *J Appl Phys* 2009;**105**, 931717-1-993717.
142. Bocher L, Aguirre MH, Logvinovich D, Shkabko A, Robert R, Trottmann M, et al. $CaMn_{1-x}Nb_xO_3$ ($x \le 0.08$) perovskite-type phases as promising new high-temperature n-type thermoelectric materials. *Inorg Chem* 2008;**47**:8077–85.
143. Tomeš P, Robert R, Trottman M, Bocher L, Aguirre MH, Bitschi A, et al. Synthesis and characterization of new ceramic thermoelectrics implemented in a thermoelectric oxide module. *J Electron Mater* 2010;**39**:1696–703.

144. Flahaut D, Funahashi R, Lee K, Ohta H, Koumoto K. Effect of the Yb substitutions on the thermoelectric properties of $CaMnO_3$. *Proc 2006 Int Conf Thermoelectrics IEEE* 2006:103–6.
145. Xu G, Funahashi R, Pu Q, Liu B, Tao R, Wang G, et al. High-temperature transport properties of Nb and Ta substituted $CaMnO_3$ system. *Solid State Ionics* 2004;**172**:147–51.
146. Lan J, Lin Y-H, Fang H, Mei A, Nan C-W, Liu Y, et al. High-temperature thermoelectric behaviors of fine-grained Gd-doped $CaMnO_3$ ceramics. *J Am Ceram Soc* 2010;**93**:2121–4.
147. Miyazaki Y, Abe D, Kajitani T. Preparation, crystal structure and thermoelectric properties of $La_{2-2x}Ca_{1+2x}Mn_2O_7$. *Proc 2006 Int Conf Thermoelectrics, IEEE* 2006:129–33.
148. Kawashima F, Huang XY, Hayashi K, Miyazaki Y, Kajitani T. Structure and high-temperature thermoelectric properties of the n-type layered oxide $Ca_{2-x}Bi_{x-\delta}MnO_{4-\gamma}$. *J Electron Mater* 2009;**38**:1159–62.
149. Lan J, Lin Y, Mei A, Nan C, Liu Y, Zhang B, et al. High-temperature electric properties of polycrystalline La-doped $CaMnO_3$ ceramics. *J Mater Sci Technol* 2009;**25**:535–8.
150. Taguchi H, Kugi T, Kato M, Hirota K. Fabrication of $(Ca_{1-x}La_x)MnO_3$ ceramics with a high relative density and their power factor. *J Am Ceram Soc* 2010;**93**:3009–11.
151. Liu C-J, Bhaskar A, Yuan JJ. High-temperature transport properties of $Ca_{0.98}RE_{0.02}MnO_{3-\delta}$ (RE = Sm, Gd, and Dy). *Appl Phys Lett* 2011;**96**:214101-1–3.
152. Cong BT, Tsuji T, Thao PX, Thanh PQ, Yamamura Y. High-temperature thermoelectric properties of $Ca_{1-x}Pr_xMnO_{3-\delta}$ ($0 \le x < 1$). *Physica B* 2004;**352**:18–23.
153. Choi S-M, Lim C-H, Seo W-S. Thermoelectric properties of the $Ca_{1-x}R_xMnO_3$perovskite system (R: Pr, Nd, Sm) for high-temperature applications. *J Electron Mater* 2011;**40**:551–6.
154. Muguerra H, Rivas-Murias B, Traianidis M, Marchal C, VanderbemdenPh, Vertruyen B, et al. Thermoelectric properties of n-type $Ca_{1-x}Dy_xMn_{1-y}Nb_yO_{3-\delta}$ compounds ($x = 0$, 0.02, 0.1 and $y = 0$, 0.02) prepared by spray-drying method. *J Alloys Compd* 2011;**509**: 7710–6.
155. Kosuga A, Urata S, Kurosaki K, Yamanaka S, Funahashi R. Mechanical properties of $Ca_{0.9}Yb_{0.1}MnO_3$/Ag composites for n-type legs of thermoelectric oxide devices. *Jpn J Appl Phys* 2008;**47**:6399–403.
156. Huang XY, Miyazaki Y, Kajitani T. High temperature thermoelectric properties of $Ca_{1-x}Bi_xMn_{1-y}V_yO_{3-\delta}$ ($0 \le x = y \le 0.08$). *Solid State Commun* 2008;**145**:132–6.
157. Park JW, Kwak DH, Yoon SH, Choi SC. Thermoelectric properties of Bi, Nb co-substituted $CaMnO_3$ at high temperature. *J Alloys Compd* 2009;**487**:550–5.
158. Cheng H, Xu XJ, Hng HH, Ma J. Characterization of Al-doped ZnO thermoelectric materials prepared by RF plasma powder processing and hot press sintering. *Ceram Int* 2009;**35**:3067–72.
159. Mele P, Matsumoto K, Azuma T, Kamesawa K, Tanaka S, Kurosaki J-I, et al. Development of Al_2O_3–ZnO/$Ca_3Co_4O_9$ module for thermoelectric power generation. *Mater Res Soc Symp Proc* 2009;**1166**:N03–23.
160. Yamaguchi H, Chonan Y, Oda M, Komiyama T, Aoyama T, Sugiyama S. Thermoelectric properties of ZnO ceramics co-doped with Al and transition metals. *J Electron Mater* 2011;**40**:723–7.
161. Ohtaki M, Tsubota T, Eguchi K, Arai H. High-temperature thermoelectric properties of $(Zn_{1-x}Al_x)O$. *J Appl Phys* 1996;**79**:1816–8.
162. Ohtaki M, Araki K, Yamamoto K. High thermoelectric performance of dually doped ZnO ceramics. *J Electron Mater* 2009;**38**:1234–8.
163. Ohtaki M, Hayashi R, Araki K. Thermoelectric properties of sintered ZnO incorporating nanovoid structure: influence of the size and number density of nanovoids. *Proc 2006 Int Conf Thermoelectrics, IEEE* 2006: 112–6.
164. Qu X, Wang W, Lv S, Ji D. Thermoelectric properties and electronic structure of Al-doped ZnO. *Solid State Commun* 2011;**151**:332–6.
165. Guilmeau E, Maignan A, Martin C. Thermoelectric oxides: effect of doping in delafossites and zinc oxide. *J Electron Mater* 2009;**38**: 1104–8.
166. Wiff JP, Kinemuchi Y, Kaga H, Ito C, Watari K. Correlations between thermoelectric properties and effective mass caused by lattice distortion in Al-doped ZnO ceramics. *J Eur Ceram Soc* 2009;**29**:1413–8.
167. Ma N, Li J-F, Zhang BP, Lin YH, Ren LR, Chen GF. Microstructure and thermoelectric properties of $Zn_{1-x}Al_xO$ ceramics fabricated by spark plasma sintering. *J Phys Chem Solids* 2010;**71**:1344–9.
168. Kinemuchi Y, Mikami M, Kobayashi K, Watari K, Hotta Y. Thermoelectric properties of nanograined ZnO. *J Electron Mater* 2010;**39**: 2059–63.
169. Park K, Seong JK, Kim GH. NiO added $Zn_{1-x}Ni_xO$ ($0 \le x \le 0.05$) for thermoelectric power generation. *J Alloys Compd* 2009;**473**:423–7.
170. Park K, Ko KY. Effect of TiO_2 on high-temperature thermoelectric properties of ZnO. *J Alloys Compd* 2007;**430**:200–4.
171. Park K, Ko KY, Seo W-S, Cho W-S, Kim J-G, Kim JY. High-temperature thermoelectric properties of polycrystalline $Zn_{1-x-y}Al_xTi_yO$ ceramics. *J Eur Ceram Soc* 2007;**27**:813–7.
172. Park K, Seong JK. Influence of simultaneous addition of Sb_2O_3 and SnO_2 on thermoelectric properties of $Zn_{1-x-y}Sb_xSn_yO$ prepared by tape casting. *J Alloys Compd* 2008;**464**:1–5.
173. Park K, Seong JK, Nahm S. Improvement of thermoelectric properties with the addition of Sb to ZnO. *J Alloys Compd* 2008;**455**:331–5.
174. Lemonnier S, Goupil C, Noudem J, Guilmeau E. Four-leg $Ca_{0.95}Sm_{0.05}MnO_3$ unileg thermoelectric device. *J Appl Phys* 2008;**104**:14505-1–4.
175. Noudem JG, Lemonnier S, Prevel M, Reddy ES, Guilmeau E, Goupil C. Thermoelectric ceramics for generators. *J Eur Ceram Soc* 2008;**28**:41–8.
176. Reddy ES, Noudem JG, Hebert S, Goupil C. Fabrication and properties of four-leg oxide thermoelectric modules. *J Phys D: Appl Phys* 2005;**38**:3751–5.
177. Funahashi R, Mikami M, Mihara T, Urata S, Ando N. A portable thermoelectric-power-generating module composed of oxide devices. *J Appl Phys* 2006;**99**:066117-1–3.
178. Funahashi R, Urata S, Mizuno K, Kouuchi T, Mikami M. $Ca_{2.7}Bi_{0.3}Co_4O_9$/$La_{0.9}Bi_{0.1}NiO_3$ thermoelectric devices with high output power density. *Appl Phys Lett* 2004;**85**:1036–8.
179. Matsubara I, Funahashi R, Takeuchi T, Sodeoka S, Shimizu T, Ueno K. Fabrication of an all-oxide thermoelectric power generator. *Appl Phys Lett* 2001;**78**:2629–3627.
180. Park K, Choi JW, Lee C-W. Characteristics of thermoelectric power modules based on p-type $Na(Co_{0.95}Ni_{0.05})_2O_4$ and n-type $Zn_{0.99}Sn_{0.01}O$. *J Alloys Compd* 2009;**486**:785–9.
181. Huang XY, Miyazaki Y, Yubuta K, Oide Y, Kajitani T. The thermoelectric properties of $[Ca_2CoO_3]_{0.62}[CoO_2]$ textured ceramics. In: *Proc 2006 Int Conf Thermoelectrics, IEEE*. 2006. p. 81–91.
182. Zhang Y, Zhang J, Lu Q. Synthesis of highly textured $Ca_3Co_4O_9$ ceramics by spark plasma sintering. *Ceram Int* 2007;**33**:1305–8.
183. Noudem JG. A new process for lamellar texturing of thermoelectric $Ca_3Co_4O_9$ oxides by spark plasma sintering. *J Eur Ceram Soc* 2009;**29**:2659–62.
184. Yoon W-H, Ryu J, Choi JJ, Hahn B-D, Choi JH, Lee B-K, et al. Enhanced thermoelectric properties of textured $Ca_3Co_4O_9$ thick film by aerosol deposition. *J Am Ceram Soc* 2010;**93**:2125–7.